

**Author response to referee comments on Chrysanthou et al. (2020) “Decomposing the response of the stratospheric Brewer-Dobson circulation to an abrupt quadrupling in CO<sub>2</sub>” submitted to Weather and Climate Dynamics Discussions**

**Reply to Anonymous Referee #1**

**General comments:**

This is an interesting, relevant and well-presented paper. The authors consider the drivers behind the response of the BDC to 4xCO<sub>2</sub> using 50-year simulations of HadGEM3. As such, the paper serves as an experimental report. The authors decompose the components of the response into those arising from rapid adjustment (holding sea-ice and SSTs constant at pre-industrial values), the global-mean SST warming (relative to pi-control), and the specific pattern of SST warming (global mean removed). I can recommend the paper for publication with a few changes as I have outlined below, none of which are particularly major and most of which just improve the readability and flow of the manuscript (to allow the science to stand out). I have a few specific comments which pertain more to the choices the authors have made in what they show/do.

Thank you for your positive comments and suggestions for improving the readability of the study. We reply to the specific points raised below in red.

**Specific comments:**

L47: I think “turnaround latitudes” needs to be briefly explained here.

Thanks for this suggestion. The first mention of the turnaround latitudes is on line 44 - we have updated the text there.

L57: I am not sure why the more general “tropical waves” is mentioned and then elaborated as “equatorially trapped quasi-stationary Rossby waves”. One is more general, while the other is more specific. Only one is necessary.

Thanks for catching this. We have kept the more general reference to tropical waves.

L140: Would it not have also been possible to perform an experiment where sea ice is allowed to vary? Comparing the results of this perturbation with those where it is held constant could show some of the possible effects on the BDC to which the authors allude is “uncertain”.

As suggested, we have performed a further simulation in which sea ice + SSTs are changed based on the multi-model mean CMIP5 4xCO<sub>2</sub> experiment. We compare this “full 4xCO<sub>2</sub> + sea-ice loss” with the full 4xCO<sub>2</sub> experiment (run B) as described in the manuscript. The annual mean  $w^*$  anomalies due to the changes in sea ice are shown below in Figure R1. This shows no significant changes in  $w^*$  due to the additional effect of sea ice loss. We have added a comment in the Methods to say we have tested the sea ice effect and it was negligible.

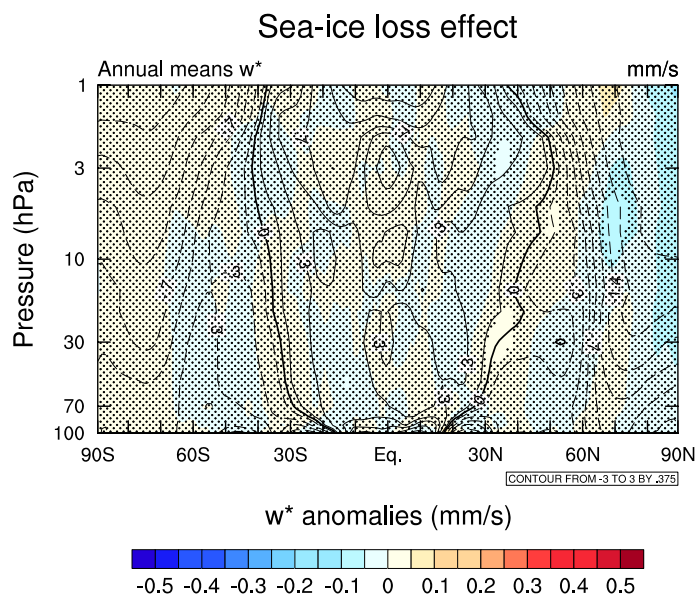


Figure R1: Annual mean  $w^*$  anomalies (mm/s) due to  $4xCO_2$  sea ice changes. Anomalies are calculated as the difference between the “full  $4xCO_2$  + sea ice loss” and “full  $4xCO_2$ ” (run B) experiments. Stippling denotes differences that are not significant at the 95% confidence level.

L242-245: This mention of changes to the QBO is tantalising! Would it be possible to include this in at least supplementary figures? This is up to the authors, and I agree it is not the focus of the study, but this mentioning of it without further information leaves me wondering what stones are unturned.

We agree this point is also interesting, but we feel it would be a separate study in its own right and that to offer enough detail to satisfactorily explain the QBO changes would detract from the main focus of the paper. We have therefore removed the mention of the changes in QBO and defer this for future study.

L403: The statement “the SST pattern imposed here is very different from a canonical ENSO SST pattern” confused me. Is it? Does this refer to the global pattern, or the tropical Pacific in particular? This seems important given what is mentioned on L90.

Thanks for pointing this out. The issue of the SST pattern was also raised by reviewer 3. On reflection the description was an oversimplification. ENSO SST anomalies are confined to the tropical Pacific, whereas the  $4xCO_2$  SST pattern shows features globally (by construction). This includes relatively higher SST across the tropical oceans and North Pacific and relatively cooler SSTs in the Southern Ocean. We have amended the text in the Methods to provide a more nuanced discussion about the features of the  $4xCO_2$  SST pattern (lines 163-165). We still discuss the BDC response to ENSO but only as a point of comparison in terms of the magnitude of its effect (tracked changes manuscript lines 461-462).

L384/Figure 10: the SST pattern effect result is non-significant (the confidence interval overlaps with 0). This should probably be mentioned.

Thank you for pointing this out. We have added this point to the text: “though the latter is not statistically distinguishable from internal variability”.

Method: What method was used to determine the 95% confidence levels? I don't think the authors have stated this.

Thank you for spotting this. The statistical significance was computed based on a two-tailed Student's t-test. We have now updated all relevant figure captions (Figures 2, 5 and 7) to include the statistical method of calculating the 95% confidence.

Results: There are cases where the individual component results are compared in a qualitative sense (e.g. L280), but it would be useful if these were sometimes more quantitative (e.g. X% more: : :) like in section 3.5.

This surely improves the comparison and brings out a more quantitative sense of the responses of all perturbations. We have now quantified the contributions of each component in the annual-mean residual circulation response (Figure 4) as well as in the seasonal mean mass streamfunction anomalies (Figures 5 and 6) in this part of the text to reflect your suggestion.

Figures: In general I did not notice that the bottom y-limit changes quite a bit between each figure, as they are all in the same format. Perhaps worth mentioning in the captions.

Thank you for pointing this out, we have now updated the relevant figure captions to note the pressure range in the y-axis.

#### **Technical corrections:**

L75: GEOS is not defined here. It is not particularly important, but it stands out as all other acronyms are.

We have added the definition for GEOS.

L90: Tilde is missing from Niño.

Thanks for this, we have now corrected it.

L90: Although it would be common to say "ENSO itself" and not "The ENSO: : :", so I understand why the authors have written it in this way, I think this sentence should begin with "THE El Niño Southern Oscillation: : :".

Thanks for this, it makes more sense to add a "The" in the beginning of the sentence.

L91: Capital H on Hemisphere (also elsewhere)

Thanks for this, we have now changed this here and in line 95.

L95: Definite article is missing " : : using THE Whole Atmosphere: : :"

Added "the" before mentioning WACCM.

L109: In the list of the components, the phrasing on (2) is slightly different to the other two, and different to how it is in the abstract which makes it 'flow' less well. Consider using the phrasing as used in the abstract "a contribution from: : :"

Thanks for this suggestion, we have now updated the text to reflect the listing of the components as seen in the abstract, as per your recommendation.

L172: Missing capital I on McIntyre (also in the references)

Thank you for spotting this, we have now corrected this.

L173: The final Andrews citation should probably be non-parenthetical “: :defined following Andrews et al. (1987): : :”

Again, thanks for spotting this, we have corrected this.

L175/equation 1: are the dots necessary? These are not consistently used in the equations shown in this paper and are not standard for scalar multiplication.

We agree that this was not consistent with the rest of the mathematical formulations of the study, so we removed the dots.

Equation 4: The integral is missing the variable of integration (dz')

Thanks for spotting this, we have now added it.

L204: “maximum” should be “maximised”, and a mention of by how much would maybe be good here

We corrected this to “maximised” and added the amount of tropospheric warming induced in that vicinity (~ 8 K).

L209: Which figure panel is run C?

This was an oversight which was corrected. Thanks!

L211-213: Is this sentence describing how the greenhouse effect works really needed?

We agree that it is redundant, so we removed it.

L230: Here, and elsewhere, additional hyphenation increases readability. For example, please revise to “annual-mean zonal-mean zonal wind”.

Thanks for this suggestion, we have corrected this here and elsewhere in the text.

L256: Insert “but small”, for “significant, but small, increases: : :”

Thank you for this suggestion, we have implemented it in the text.

L263 & 266 & 267: Why is Hardiman et al. cited for results that are in the figures? If it is to say that the result is consistent, then please state as such.

We have removed these citations.

L272: Consider changing  $p < 10$  hPa to “below 10 hPa” for readability.

Thanks for this suggestion, we have updated the text.

L310: Eliassen-Palm Flux is earlier abbreviated to EPF.

We have now corrected this, thanks.

L405-410: “important role” and “decomposition performed here” and both repeated twice in the same paragraph. Consider revising one of each to a different phrase.

We have altered the second sentence to reflect your suggestion, which now reads: *“However, our results demonstrate that an increase of the BDC in the upper stratosphere comes mainly from the radiative cooling of the stratosphere by CO<sub>2</sub>, as seen in the rapid adjustment component of the response”*

L437: “the projection reduction” should be “the projected reduction”

Nice catch, thanks.

L634: This reference has two hyperlinks.

We removed the additional hyperlink, thanks.

L637: Is this cited in the text? NCL is credited in the acknowledgments but is not linked to this reference.

It was only cited in the acknowledgments however the bibliography entry was wrong, thanks for spotting it. We have now corrected this.

Figure 1: For (b), some specification that the contour value is 3.4 K would be helpful.

Thank you for this, we have now added a string on Fig. 1b that states the value of the constant contour value of 3.4 K. The colour of the contour reflects the colormap of Fig. 1a.

Figure 2 (and similar): It would be helpful if the figures had the experiment labels on them, or in the caption, as this can get confusing.

Thank you for this suggestion. We have updated with the experiment labels the captions of all related figures to clarify which panel corresponds to which experiment.

Figure 6: This shows EP flux vector ANOMALIES which is not stated in the caption.

We appreciate that you spotted this, we now state that these are the EPF vector anomalies in the newly added DJF-mean Figure 7 caption.

## Author response to referee comments on Chrysanthou et al. (2020) “Decomposing the response of the stratospheric Brewer-Dobson circulation to an abrupt quadrupling in CO<sub>2</sub>” submitted to Weather and Climate Dynamics Discussions

### Reply to Anonymous Referee #2

This study is on the changes in the stratospheric Brewer-Dobson circulation in response to a quadrupling of CO<sub>2</sub> concentration. Utilizing the HadGEM3-A model, the authors separate out the fast response to CO<sub>2</sub> increase from the effect of uniform SST warming as well as the SST warming pattern. It is found that the uniform warming dominates the circulation changes in the lower stratosphere, but the rapid adjustment makes comparable contribution to the uniform warming at the 10 hPa. This is a useful study in understanding the climate changes in the stratosphere. The manuscript is generally well written and logically organized. I have some relatively minor comments on some of the results and discussion and would recommend publication after the authors address these comments.

We appreciate your constructive comments in order to improve the results and discussion of the study. We reply to the specific points raised below in red.

#### Main comments:

1. The mechanism for the rapid adjustment of the BDC. Can the authors elaborate a little more on how the rapid adjustment affect the BDC? The authors briefly mentioned the radiative cooling in the stratosphere. One possibility is that the radiative cooling then affects the strength of the polar night jet via thermal wind balance, which then affect wave dissipation and the BDC. However, the rapid adjustment of the zonal wind shows weak decrease in the NH upper stratosphere and moderate increase in the SH upper stratosphere (Fig. 3b). Such wind changes seem to be inconsistent with the changes in  $w^*$  (Fig. 4b), which shows large strengthening of the downwelling over the Arctic and small strengthening over the Antarctic.

Thanks for this interesting comment. The thermal wind response due to the direct cooling is fairly small because the CO<sub>2</sub> radiative cooling is quite homogeneous in latitude (Fels et al., 1980). One hypothesis that we think is plausible is that the radiative cooling alters the refractive index in the stratosphere, which changes the propagation and breaking of Rossby waves. The refractive index,  $n_r$ , is dependent on the Brunt-Väisälä frequency (e.g., Matsuno, 1970),  $N^2$ , which is in turn related to the vertical gradient of potential temperature:

$$N^2 = \frac{g}{\theta} \frac{d\theta}{dz}$$

Hence the stratospheric cooling, which increases with height, alters  $N^2$  and in turn  $n_r$ . Unfortunately, we do not have the model variables to calculate  $n_r$  directly for the simulations. We have added a section discussing this possible mechanism (revised manuscript lines 350 – 359 / tracked changes manuscript lines 383-391):

“Previous studies have demonstrated mechanisms for tropospheric warming to influence the stratospheric EPFD and residual circulation (e.g., Shepherd and McLandress, 2011), but the mechanism through which the rapid adjustment acts on EPFD in the upper stratosphere is less well understood. The radiative cooling in the stratosphere due to increased CO<sub>2</sub> is relatively uniform in latitude (Fels et al., 1980), so we do not expect large direct changes in zonal wind through thermal wind balance. However, the temperature response to CO<sub>2</sub> represents a weakening of the vertical temperature gradient, particularly in the upper stratosphere where the cooling is larger. The characteristics for wave propagation and refraction can be

quantified using a measure of refractive index (e.g., Matsuno, 1970) that is dependent on the Brunt-Väisälä frequency ( $N_2 = g/\theta(d\theta/dz)$ ). Hence, we hypothesise that the changes in background temperature structure due to the CO<sub>2</sub> radiative effects alter the propagation of Rossby waves, particularly in the upper stratosphere, and this leads to the changes in EPFD shown in Figures 7 and 8.”

2. The EP flux divergence plots seem to be inconsistent with the changes in stream function. The downward control principle indicates that the latitudinal distribution of  $\Psi^*$  anomalies should be roughly consistent with those of EP flux divergence anomalies. However, the EP flux divergence anomalies seems to locate much poleward than  $\Psi^*$  anomalies, especially in DJF over the Southern Hemisphere (Fig. 6 vs. Fig. S1, Fig. 7 vs. Fig. S2). Based on the argument that stronger subtropical jets following warming allow more waves penetrate into the stratosphere, one would expect the anomalous wave dissipation to occur at the subtropics. This also seems to disagree with the pattern shown in Fig. 6 and 7, where maximum wave dissipation occurs around 50-60 degrees.

The torque exerted on the zonal flow and the associated  $w^*$  anomalies is proportional to  $EPFD \times \cos(\text{lat})$  (Haynes et al., 1991); this explains the apparent difference in pattern of EPFD and  $\psi^*$ . When the EPFD is multiplied by  $\cos(\text{lat})$  the patterns more strongly resemble one another (see Figure R1 below), as expected. Furthermore, this weighted pattern of EPFD anomalies compares closely with the distribution of wave forcing found by Shepherd and McLandress, (2011) who showed in detail the role of changing Rossby wave critical lines in the subtropical lower stratosphere. We have replaced Figures 6 and 7 of the main text with the below figures which show the cosine(latitude) weighted EPFD anomalies. We have also replotted the parametrized wave forcing supplementary figures using the same scaling.

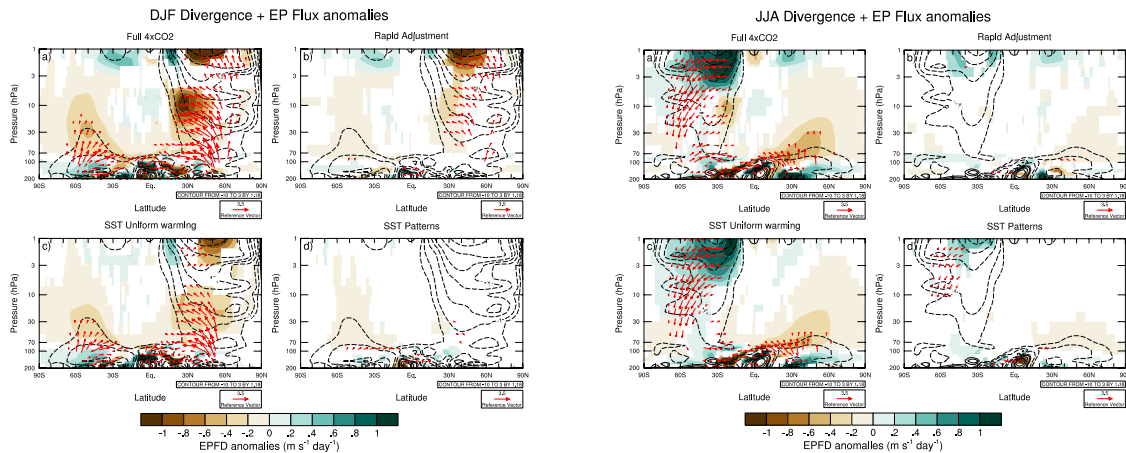


Figure R1: (left) As in Figure 6 of the main text, showing DJF EPFD anomalies for the four experiments, but multiplied by cosine of latitude. (right) As in Figure 7 of main text, showing JJA EPFD anomalies.

3. Model bias in climatology. The model simulated turn-around latitude in piControl climatology seems to be too poleward compared to reanalysis or other models (e.g., Fig. 1 in Hardiman et al. (2014)). At around 20 hPa, there are multiple turn-around latitude in the Northern Hemisphere, indicating more than one cell of the circulation, which seems unreasonable. Such bias in the mean circulation structure reflects bias in the waves forcing and/or other background condition. Would such model bias affect the model’s ability to simulate the circulation changes in response to CO<sub>2</sub> increase?

To further investigate this feature in the turnaround latitudes, Figure R2 below shows the  $w^*$  anomalies and turnaround latitudes by season. This shows the feature in the NH midlatitude middle stratosphere is a feature of the DJF season. There is a similar but less pronounced feature in the SH in JJA. We agree that, like any model, HadGEM3 contains biases which may affect the specific results of the study. However, we emphasise that the overall simulated changes in residual circulation correspond very well with other studies analysing large forced changes in the BDC in a range of climate models (e.g., Shepherd and McLandress, 2011; Hardiman et al., 2014; Lin et al., 2015). We have added a sentence at the end of the conclusions caveating that the results are from one model and that climatological biases might affect its simulation of the forced response to CO<sub>2</sub>: “The model contains mean biases that could affect some of the details of the responses described here.”

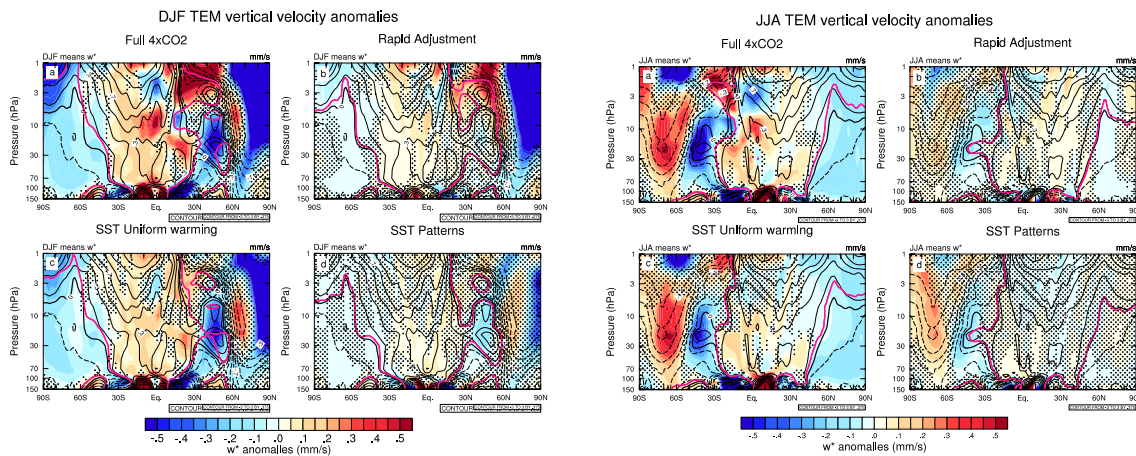


Figure R2: As in Figure 4 of the main text, showing  $w^*$  anomalies in the experiments and the turnaround latitudes, but for (left) DJF and (right) JJA seasons.

**Other minor comments and typos:**

Line 152-155: experiment “A, C, B, D” should be “B, D, C, E”.

Thanks for spotting these typos. We have now corrected the experiment labels mentioned in this part.

Line 281-282: It is hard to compare the three components over NH extratropical middle and upper stratosphere in Fig. 5, as they all seem to be less than the contour interval. On the other hand, the  $w^*$  changes shown in Fig. 4 seem to suggest that the SST pattern effect is much weaker than the uniform warming or the rapid adjustment.

We have added additional contour intervals to resolve the upper stratospheric anomalies.

Line 330: Fig. 7b should be Fig. 7c.

Thanks for pointing this out, we have now corrected it.

**References**

Fels, S. B., Mahlman, J. D., Schwarzkopf, M. D. and Sinclair, R. W.: Stratospheric Sensitivity to Perturbations in Ozone and Carbon Dioxide: Radiative and Dynamical Response, Journal of the

Atmospheric Sciences, 37(10), 2265–2297, doi:10.1175/1520-0469(1980)037<2265:SSTPIO>2.0.CO;2, 1980.

Hardiman, S. C., Butchart, N. and Calvo, N.: The morphology of the Brewer-Dobson circulation and its response to climate change in CMIP5 simulations, *Quarterly Journal of the Royal Meteorological Society*, 140(683), 1958–1965, doi:10.1002/qj.2258, 2014.

Haynes, P. H., McIntyre, M. E., Shepherd, T. G., Marks, C. J. and Shine, K. P.: On the “Downward Control” of Extratropical Diabatic Circulations by Eddy-Induced Mean Zonal Forces, *Journal of the Atmospheric Sciences*, 48(4), 651–678, doi:10.1175/1520-0469(1991)048<0651:OTCOED>2.0.CO;2, 1991.

Lin, P., Ming, Y. and Ramaswamy, V.: Tropical climate change control of the lower stratospheric circulation, *Geophysical Research Letters*, 42(3), 941–948, doi:10.1002/2014GL062823, 2015.

Matsuno, T.: Vertical Propagation of Stationary Planetary Waves in the Winter Northern Hemisphere, *Journal of the Atmospheric Sciences*, 27(6), 871–883, doi:10.1175/1520-0469(1970)027<0871:vpospw>2.0.co;2, 1970.

Shepherd, T. G. and McLandress, C.: A Robust Mechanism for Strengthening of the Brewer–Dobson Circulation in Response to Climate Change: Critical-Layer Control of Subtropical Wave Breaking, *Journal of the Atmospheric Sciences*, 68(4), 784–797, doi:10.1175/2010JAS3608.1, 2011.

**Author response to referee comments on Chrysanthou et al. (2020) “Decomposing the response of the stratospheric Brewer-Dobson circulation to an abrupt quadrupling in CO<sub>2</sub>” submitted to Weather and Climate Dynamics Discussions**

**Reply to Anonymous Referee #3**

Changes in the Brewer-Dobson circulation (BDC) due to increased CO<sub>2</sub> levels are studied by distinguishing the response to CO<sub>2</sub> changes in the atmosphere only, globally uniform changes in SSTs, and SST pattern changes. The former corresponds to the rapid-adjustment of the climate system when CO<sub>2</sub> levels are increased abruptly. The latter two correspond to long-term changes due to the longer time scales of the oceanic response. These effects are studied consistently by using a single state-of-the-art climate model (HadGEM3-A). The BDC generally increases in strength due to increased CO<sub>2</sub>. The authors find that in the lower stratosphere the majority of this BDC strengthening can be attributed to globally uniform SST increase. In the upper stratosphere the changes due to rapid adjustment are of similar magnitude. The authors furthermore estimate a linear sensitivity of the change in BDC strength as a function of global surface warming of roughly 9 %/K in the lower stratosphere and 6 %/K in the upper stratosphere. Overall, the paper is well-written and the results are straightforward. I have a few general comments that I hope will help the authors to sharpen their discussion and to better put the work into broader context. Other than that I only have minor comments; once these comments have been taken into account this manuscript should be publishable.

Thank you for your positive comments and suggestions to sharpen the discussion and enhance the readability of the study. We reply to the specific points raised below in red.

**General comments:**

SST pattern changes and ENSO: there are frequent remarks about the resulting BDC changes from the SST pattern changes to be similar to ENSO-induced anomalies. However, in the discussion section (line 403) the authors remark that "the SST pattern imposed here is very different from a canonical ENSO SST pattern". If that is the case, isn't it surprising then that the BDC changes due to the SST pattern changes look similar to those due to ENSO? To me this calls for corresponding discussion/elaborations somewhere in the manuscript.

Thanks for the comment. The issue of the pattern was also raised by reviewer 1. On reflection this description was an oversimplification. ENSO SST anomalies are confined to the tropical Pacific, whereas the 4xCO<sub>2</sub> SST pattern shows features globally (by construction). This includes relatively higher SST across the tropical oceans and North Pacific and relatively cooler SSTs in the Southern Ocean. We have amended the text in the Methods to provide a more nuanced discussion about the features of the 4xCO<sub>2</sub> SST pattern (lines 163-165). We still discuss the BDC response to ENSO but only as a point of comparison in terms of the magnitude of its effect (tracked changes manuscript lines 461-462).

Shallow versus deep branch changes: it seems that the authors interpret changes in upwelling strength through 70 hPa as representative of the shallow BDC branch, whereas those at 10 hPa as representative of the deep branch. Although it is certainly true that there isn't a clear vertical level where the shallow branch stops and the deep branch takes over, perhaps a useful distinguishing factor is related to the tropical pipe concept (much less meridional exchange at pressure levels within the tropical pipe than below). The shallow branch could then be interpreted as being primarily confined to that part of the BDC that involves strong meridional dispersion below the bottom of the tropical pipe. My recollection is that this level (bottom of tropical pipe) is close to 70 hPa, although this may vary from model to model. By that argument the upwelling through 70 hPa is more a measure of the deep rather than the shallow BDC branch and neither

of the quoted upwelling changes correspond to the shallow branch strength. I admit that all of this may be a bit philosophical, but the authors may wish to include a bit of discussion on this point. This isn't an issue when simply referring to 70 vs. 10 hPa without the connotation of shallow vs. deep branch. But even in that case, one wonders about BDC changes in the lower half of the stratosphere (assuming a global mean tropopause pressure somewhere around 150 hPa, roughly half of the stratosphere is located below 70 hPa)

We agree there is no accepted pressure level to delineate the different branches of the BDC, that different levels have been used throughout the literature, and that these levels likely vary in models too. Our choice of levels to focus on was partly motivated by the comparison with earlier model intercomparisons (e.g., Fig 4.10 SPARC, 2010), which tended to analyse the BDC at 70 hPa and 10 hPa. For clarity, we have amended the text to always refer to the specific pressure levels and/or to the lower and upper stratosphere rather than to the shallow and deep branches. Based on the reviewer's points about the mass flux in the lower stratosphere, we have also amended our cross-section plots to show levels down to 150 hPa.

Seasonal versus annual means: residual circulation changes are shown in terms of annual means in the main manuscript, whereas those of EP flux divergence are shown in terms of seasonal means. Line 308 presents a specific argument in favour of seasonal means. I didn't understand why this argument should apply to the wave forcing but not the resulting residual circulation, hence why seasonal means were delegated to the supplement in the case of the residual circulation? Please clarify somewhere.

Following this comment, we have moved the seasonal mean  $\psi^*$  Figures S1 and S2 to the main text and moved the annual mean  $\psi^*$  in Fig. 5 to the supplement. This part of the manuscript was rewritten to reflect the above changes.

#### **Minor comments:**

line 47: not sure I can follow the argument here - why couldn't the wave forcing around the turnaround latitudes change if there was a change in wave activity from the troposphere?

This sentence was indeed misleading. We meant that the wave forcing *change* needs to take place near the turnaround latitudes (TL) to directly affect the BDC. Poleward of the TL and within the deep tropics it will only lead to a latitudinal re-distribution of the downwelling or upwelling respectively (Shepherd and McLandress, 2011). We have updated the text to clarify this point.

line 51: the Randel and Held reference is appropriate for the connection of wind pattern and critical levels, but I don't think these authors talked about an upward movement of critical levels due to climate change; so the placement of this reference may be misleading

Indeed, the placement of this reference was misleading, so we have now removed it. We added a new sentence to better put into context the observed link between the wind patterns and the critical levels of wave breaking associated with an accelerated BDC under climate change.

line 81: GEOS-CCM model: the acronym "CCM" already contains "model"

Thanks for spotting this, we have now removed the word "model".

line 88: here and at other place: "warmer SSTs" should be something like "higher SSTs" (or "warmer sea surfaces")

Following your suggestion, we have changed the warmer SSTs to "higher" SSTs.

line 106: "three distinct effects" – would be good to briefly remind reader about the effects

This suggestion surely improves the readability in this part of the manuscript, so we briefly list these effects. Thanks!

line 144: is the runtime for the 4xCO<sub>2</sub> experiments long enough to call the final state "quasi-equilibrium"? I could imagine that there's still drift due to ocean response, even after 150 years.

The reviewer is correct that the climate has not fully equilibrated after 150 years. We have removed the phrase "quasi-equilibrium" and replaced it with "centennial".

line 147/148: please add comment about the 3.4 K warming, especially comparing it to the equilibrium response to 4xCO<sub>2</sub> (which should be double the climate sensitivity if I understand correctly, so the 3.4 K value seems small)

This value is not comparable to the equilibrium climate sensitivity (ECS), since this is the global surface temperature (land+ocean) and we consider only the global mean SST change. Since the land warms more than the ocean, we expect our imposed global SST change to be smaller than 2xECS. Furthermore, our warming is calculated over years 101-150 whereas ECS extrapolates to equilibrium which takes millennia to reach (Rugenstein et al., 2020). We have added a comment in the Methods on this point: "Note the global mean SST is smaller than the global mean surface temperature change in the abrupt-4xCO<sub>2</sub> experiment because land areas warm more than the ocean (e.g., Joshi and Gregory, 2008)."

line 175 and following: please clarify use of vertical coordinate; your model runs in height coordinates (not log-p height), but the TEM diagnostics are formulated in log-p height – was this done by first interpolating the data?

Thank you for spotting this, the equations were incorrectly written in the log-p coordinate system although the MetUM uses the primitive equations with the log-pressure  $z = -H \ln(p/ps)$  coordinate. We did not perform any interpolation; we used the direct model output which was calculated based on the equations 3.5.1a and 3.5.1b from Andrews et al., (1987).

line 181: I assume that Eq. 2 is only integrated to the respective vertical level of interest (so that  $\Psi^*$  is still function of log-p height), not all the way to the surface (unless for lowest level)? Also, your definitions in Eqs. 1 and 2 are circular: Eq. 1 requires knowledge of  $\Psi^*$  and Eq. 2 requires knowledge of  $v^*$  ... even though these are standard diagnostics, it would be more helpful to define the residual streamfunction first based on the vertically integrated  $v$  and the heat flux contribution; then define  $v^*$  and  $w^*$  (or, alternatively, define  $v^*$  and  $w^*$  in terms of  $v$  and  $w$  + heat flux contribution; then use Eq. 2 for  $\Psi^*$ ).

For the first part of the question, yes for each level, we integrate from the top of the model to that particular level. Following up from your previous comment, we now define the residual circulation equations as shown in Andrews et al., (1987), changing our equation 1 and keeping equation 2 as it is in the manuscript. We have also updated the text to reflect these changes.

Eq. 4: the integral is missing a "dz"

Thanks for spotting this, we have now added it.

line 244: please make more definite statements about the direction of changes of these QBO characteristics (or omit the comment altogether)

We feel it would be a separate study in its own right and that to offer enough detail to satisfactorily explain the QBO changes would detract from the main focus of the paper. We have therefore amended the text: “This is likely related to changes to the QBO properties under climate change, which have been noted in other idealised GCM experiments (e.g. Kawatani et al., 2011), though a detailed investigation of the QBO is beyond the scope of this study”.

line 259: this is a good example where you make a reference to ENSO-like SST perturbations, but fall short in discussing how your SST pattern changes actually do correspond to ENSO (or not)

Thanks for pointing this out. The issue of the pattern was also raised by reviewer 1. While the SST pattern shows an El Niño-like warming across the equatorial Pacific, the pattern shows other pronounced features such as relatively warmer SSTs across all tropical ocean basins and the North Pacific and relatively cooler SSTs across the Southern Ocean. We have clarified the text on the SST pattern and its interpretation in relation to the local tropical Pacific anomalies vs. the global pattern.

line 263: this is a good example where I found your reference to the shallow BDC branch confusing – to me it doesn't really extend to 30 hPa

We have reworded the text to make this clearer.

lines 299/300: should this result perhaps be shown / referred to right away with the methods section? Also: it sounds a bit misleading to me to start the paragraph with "An important question" and then talk about results shown in the supplement – if they really are important, why aren't they shown in the main part of the paper?

We prefer to place this discussion here because it follows from the detailed discussion of the individual responses and would therefore be premature in the Methods. We have reworded the opening phrase of the paragraph from “An important question...” to “We lastly consider...”.

line 330: SSW -> SST

Thank you for spotting this, we have now corrected it.

line 350: could you elaborate where this 20 % disagreement could come from?

The direct  $\psi^*$  calculation is derived from  $v^*$  (see Equation 2). This was used because it was found to be less noisy than performing an equivalent integration of  $w^*$  in latitude. However, in previous work we have noticed that, for model pressure level data, the  $\psi^*$  estimated from  $v^*$  is generally larger than that from  $w^*$  (see Fig. S2 of Dietmüller et al., 2018). We hypothesise that this is the source of the difference between the direct and downward control calculations, though we cannot explain its origin. We have added a reference to this in the text.

line 400: the statement is based on results from this paper, so I assume the reference to Lin et al. is meant to state that they found similar results? Please clarify

Thanks for spotting this, this was referring to the fact that the Lin et al., (2015) study had similar findings. We have slightly updated the text to better communicate this.

line 434: this value ( $\sim 9$  %/K) is exactly equal to the one you quote for your results, so the agreement is exact (or almost exact) and not just "relatively good" - am I missing something?

Thank you for pointing this out, as a matter of fact it is in exact agreement. We have now updated the text to reflect this.

line 675 (Fig. 3 caption): the  $u=0$  lines are only critical lines for stationary waves - please clarify

Thank you for bringing this to our attention. We now clarify that the critical lines refer to stationary waves.

Fig. 4 and related discussions: visually, it doesn't look like the positive anomalies compensate the negative anomalies on a given pressure level (perhaps when scaled by surface area they do), but shouldn't they based on mass conservation? Did you check?

Yes, we have verified that the  $\cos(\text{latitude})$  area weighted  $w^*$  anomalies on a given pressure surface produce a very small residual, e.g. at 70 hPa the area average value is  $-0.013$  mm/s for the full experiment (annual mean), which is around 20 times smaller than the magnitude of anomalies at individual latitudes.

## References

Andrews, D. G., Leovy, C. B., Holton, J. R. and Leovy, C. B.: Middle Atmosphere Dynamics, Academic press., 1987.

Dietmüller, S., Eichinger, R., Garny, H., Birner, T., Boenisch, H., Pitari, G., Mancini, E., Visioni, D., Stenke, A., Revell, L., Rozanov, E., Plummer, D. A., Scinocca, J., Jöckel, P., Oman, L., Deushi, M., Kiyotaka, S., Kinnison, D. E., Garcia, R., Morgenstern, O., Zeng, G., Stone, K. A. and Schofield, R.: Quantifying the effect of mixing on the mean age of air in CCMVal-2 and CCMI-1 models, *Atmospheric Chemistry and Physics*, 18(9), 6699–6720, doi:10.5194/acp-18-6699-2018, 2018.

Joshi, M. and Gregory, J.: Dependence of the land-sea contrast in surface climate response on the nature of the forcing, *Geophysical Research Letters*, 35(24), L24802, doi:10.1029/2008GL036234, 2008.

Kawatani, Y., Hamilton, K. and Watanabe, S.: The Quasi-Biennial Oscillation in a Double CO<sub>2</sub> Climate, *Journal of the Atmospheric Sciences*, 68(2), 265–283, doi:10.1175/2010JAS3623.1, 2011.

Lin, P., Ming, Y. and Ramaswamy, V.: Tropical climate change control of the lower stratospheric circulation, *Geophysical Research Letters*, 42(3), 941–948, doi:10.1002/2014GL062823, 2015.

Rugenstein, M., Bloch-Johnson, J., Gregory, J., Andrews, T., Mauritsen, T., Li, C., Frölicher, T. L., Paynter, D., Danabasoglu, G., Yang, S., Dufresne, J., Cao, L., Schmidt, G. A., Abe-Ouchi, A., Geoffroy, O. and Knutti, R.: Equilibrium Climate Sensitivity Estimated by Equilibrating Climate Models, *Geophysical Research Letters*, 47(4), 1–12, doi:10.1029/2019GL083898, 2020.

Shepherd, T. G. and McLandress, C.: A Robust Mechanism for Strengthening of the Brewer–Dobson Circulation in Response to Climate Change: Critical-Layer Control of Subtropical Wave Breaking, *Journal of the Atmospheric Sciences*, 68(4), 784–797, doi:10.1175/2010JAS3608.1, 2011.

SPARC: SPARC CCMVal Report on the Evaluation of Chemistry-Climate Models. V. Eyring, T. Shepherd and D. Waugh (Eds.), SPARC Report No. 5, WCRP-30/2010, WMO/TD-No.40 [online] Available from: <http://www.sparc-climate.org/publications/sparc-reports/sparc-report-no5/>, 2010.

# Decomposing the response of the stratospheric Brewer-Dobson circulation to an abrupt quadrupling in CO<sub>2</sub>

Andreas Chrysanthou<sup>1</sup>, Amanda C. Maycock<sup>1</sup> and Martyn P. Chipperfield<sup>1</sup>

<sup>1</sup> School of Earth and Environment, University of Leeds, Leeds, LS2 9JT, UK

**Correspondence:** Andreas Chrysanthou ([ccac@leeds.ac.uk](mailto:ccac@leeds.ac.uk))

**Abstract.** We perform ~~50-year long~~ time-slice experiments using HadGEM3-A to decompose the long-term (years 101-150) response of the Brewer-Dobson circulation (BDC) to an abrupt quadrupling in CO<sub>2</sub> (4×CO<sub>2</sub>) into: 1) a rapid atmospheric adjustment; 2) a contribution from the global-average sea surface temperature (SST) change (+3.4 K); and 3) an SST pattern effect. The SST fields are derived from the CMIP5 multi-model ensemble. Two further experiments explore the impact on the BDC of the spread in global-average SST response to 4×CO<sub>2</sub> across the CMIP5 models (range 2.1-4.9 K). At 70 hPa (10 hPa) the annual-mean tropical upward mass flux increases by 45% (35%) due to the 4×CO<sub>2</sub> perturbation. At 70 hPa, around 70% of the increase is from the global-uniform SST warming, with the remainder coming in similar contributions from the rapid adjustment and SST pattern effect. In contrast, at 10 hPa the ~~increase in total~~ mass flux ~~increases by 35% and~~ comes mainly from the rapid adjustment (~40%) and the uniform SST warming (~45%), with a small contribution from the SST pattern. ~~Therefore, a~~At 10 hPa, the ~~magnitude~~effect of the ~~multi-model~~ spread in global-uniform-mean SST ~~response~~ is comparable in ~~magnitude~~ to the rapid adjustment. Conversely, at 70 hPa the effect of spread in global-mean SST is ~~substantially~~ larger than both the rapid adjustment and the SST pattern effect. We derive an approximately linear sensitivity of the tropical upward mass flux to global surface air temperature change of  $0.62 \times 10^9 \text{ kg s}^{-1} \text{ K}^{-1}$  (9% K<sup>-1</sup>) at 70 hPa and  $0.10 \times 10^9 \text{ kg s}^{-1} \text{ K}^{-1}$  (6% K<sup>-1</sup>) at 10 hPa. The results confirm the most important factor for the acceleration of the BDC in the lower stratosphere under increased CO<sub>2</sub> is global SST changes. We also quantify for the first time that the rapid adjustment to CO<sub>2</sub> is of similar importance to SSTs for the increased BDC in the upper stratosphere. This demonstrates a potential for a fast and slow timescale of the response of the BDC to greenhouse gas forcing, with the relative prominence of those timescales being height dependent.

## 1 Introduction

The residual circulation in the stratosphere, or the Brewer–Dobson circulation (BDC), is characterised by slow ascent in the tropics, poleward flow and downwelling in the subtropics and extratropics (Andrews et al., 1987; Holton et al., 1995; Plumb, 2002). There is a strong seasonality in the strength and width of the BDC (Rosenlof, 1995). In the winter hemisphere, the poleward mass transport that occurs in the middle and upper stratosphere is termed the deep branch, while the shallow branch in the lower stratosphere is present year-round in both hemispheres (Birner and Bönisch, 2011). The BDC controls the transport and distribution of radiatively active trace gases such as stratospheric ozone and water vapour (Brewer, 1949; Dobson, 1956), as well as the lifetimes of chemically important trace gases such as chlorofluorocarbons (CFCs; Butchart and Scaife, 2001).

The BDC is a wave-driven circulation forced by breaking of planetary-scale Rossby waves and small-scale gravity waves (Holton et al., 1995). The torque imposed by the wave breaking allows flow across lines of constant angular momentum.

General circulation models (GCMs) and chemistry-climate models (CCMs) consistently simulate an acceleration of the BDC in scenarios that include increasing greenhouse gas concentrations (Rind et al., 1990, 2002; Sigmond et al., 2004; Butchart et al., 2006, 2010; Fomichev et al., 2007; Olsen et al., 2007; Deckert and Dameris, 2008; Garcia and Randel, 2008; Li et al., 2008; Calvo and Garcia, 2009; McLandress and Shepherd, 2009; Oman et al., 2009; SPARC, 2010; Garny et al., 2011; Shepherd and McLandress, 2011; Lin and Fu, 2013; Hardiman et al., 2014). A strengthened BDC increases stratosphere-troposphere exchange (STE) of ozone (Rind et al., 2001; Hegglin and Shepherd, 2009; Banerjee et al., 2016) and affects projected ozone trends in the tropical lower stratosphere (e.g. Keeble et al., 2017), subtropics (e.g. Li et al., 2009), and polar regions (e.g. Oman et al., 2009).

The wave forcing that drives the BDC arises from various types of waves generated in the troposphere with different temporal and spatial scales (e.g., Randel et al., 2008), which propagate upwards, break and dissipate their momentum and energy (Holton et al., 1995; Plumb and Eluszkiewicz, 1999; Semeniuk and Shepherd, 2001). Changes in the BDC must, therefore, be accompanied by changes in stratospheric wave forcing. Three main mechanisms for the altered wave forcing of the BDC under climate change have been considered in the literature: 1) changes in the strength of tropospheric wave generation; 2) changes in the latitudinal distribution of wave forcing within the stratosphere in the vicinity of the turnaround latitudes, ~~where the residual vertical velocity changes sign, which separate~~ the areas of tropical upwelling ~~and~~ from extratropical downwelling; and 3) changes in the vertical penetration of tropospheric wave forcing into the stratosphere. Anomalous wave activity emanating from the extratropical troposphere has been shown to have a minimal impact on the overall strength of the BDC ~~because it generally does not induce a torque in the vicinity of the turnaround latitudes~~ (Butchart and Scaife, 2001; Sigmond et al., 2004; Garcia and Randel, 2008; Garny et al., 2011) ~~owing to the fact the wave forcing needs to occur in the vicinity of the turnaround latitudes.~~

Many studies have pointed to an important role for the projected strengthening and upward shift of the subtropical jets with tropospheric warming to explain ~~the~~ modelled increases in the BDC under climate change. ~~Rosby wave breaking regions such as the upper flanks of the subtropical jets generally follow critical layers as demonstrated by the observational study of Randel and Held (1991). This~~ robust change in the pattern of zonal winds ~~under climate change~~ (Collins et al., 2013) moves the Rossby wave critical layers in the lower stratosphere upward ~~(Randel and Held, 1991)~~, enabling enhanced penetration of Rossby wave activity in the subtropical lower stratosphere and an altered distribution of momentum deposition (Rind et al., 1990; Garcia and Randel, 2008; McLandress and Shepherd, 2009; Calvo and Garcia, 2009; Garny et al., 2011). ~~In support of~~ ~~Consistent with~~ this theoretical basis, the multi-model spread in the end of 21<sup>st</sup> century lower stratospheric zonal wind trends near the turnaround latitudes was found to explain ~70% of the spread in tropical upward mass flux trends in the lower stratosphere across a set of CCMs (Lin and Fu, 2013). Some studies have also found a role for enhanced excitation of tropical waves ~~(equatorially trapped quasi-stationary Rossby waves)~~ under climate change for a strengthened BDC (Deckert and

60 Dameris, 2008; Calvo and Garcia, 2009), but the potential for this to drive an increase in the total mass circulation rather than simply a redistribution within the tropics has been questioned (Garny et al., 2011; Shepherd and McLandress, 2011).

Although the signal of an increased BDC in a warmer climate is a highly robust feature of GCMs and CCMs, there are differences amongst models in the relative contributions to the increase from resolved and parameterized wave forcing (Butchart et al., 2006, 2010; Garcia and Randel, 2008; Calvo and Garcia, 2009; McLandress and Shepherd, 2009; Garny et al., 65 2011). This may be related to models having different climatological resolved and parameterized wave forcing (e.g., Chrysanthou et al., 2019) and/or the potential for a compensation effect between the different types of wave forcing in driving a change in the BDC (e.g. Cohen et al., 2013; Sigmond and Shepherd, 2014).

To understand the relative importance of different drivers, some modelling studies have performed idealised experiments to decompose the BDC response to climate change into different components. Sigmond et al. (2004) performed experiments 70 with the Canadian Middle Atmosphere Model (CMAM) in which CO<sub>2</sub> was doubled separately in the troposphere and stratosphere. In each case, sea surface temperature (SST) changes were imposed as a fraction of the total SST response according to their respective radiative forcings. Sigmond et al. (2004) showed that the increase in residual circulation in DJF caused a small warming in the Arctic lower stratosphere, of which about two thirds could be attributed to the tropospheric CO<sub>2</sub> doubling and about one third to the middle-atmospheric CO<sub>2</sub> doubling. Their results were qualitatively consistent with the 75 seminal results of Rind et al. (1990) who performed comparable experiments with the NASA Goddard Institute for Space Studies (GISS) model but over a shorter period.

Olsen et al. (2007) performed experiments for the period 1949 to 1998 with the NASA ~~Goddard Earth Observing System,~~ 80 ~~version 4 (GEOS-4)~~ GCM using prescribed observed SSTs. They attributed the increase in residual circulation between the first and last decades of their simulations to a stronger SST gradient between the tropics and middle latitudes, resulting in a greater meridional temperature gradient in the subtropical troposphere and more poleward refraction of planetary-scale Rossby waves in the lower stratosphere. Further simulations by Olsen et al. (2007) added the radiative effects of atmospheric GHG changes and showed a small but insignificant increase in STE trend compared to the SST-only experiments. Oman et al. (2009) performed sensitivity experiments with the GEOS-CCM ~~model~~ (based on GEOS-4) to decompose the relative effects of SSTs, 85 GHGs and halogens on the stratospheric age of air distribution between 1960 and 2100. To isolate the effects of SST changes, they compared simulations using SSTs from two different climate models that differed in their climatological SST. They describe the SST experiment as “tropical SSTs” though the SST changes appear to be imposed globally. This comparison further combines the effects of differences in both global mean SST and SST patterns between the two climate model datasets, though this was not explicitly discussed. As with all other similar studies, they concluded that increased SSTs contribute to an increase in tropical lower stratospheric upwelling and a decrease in age of air.

90 While studies have demonstrated that ~~warmer~~ ~~higher~~ SSTs increase the strength of the BDC (Olsen et al., 2007; Oman et al., 2009; Lin et al., 2015), one confounding factor ~~in the literature~~ is that the SST response to ~~climate change~~ ~~anthropogenic forcing shows an inhomogeneous pattern~~ (e.g., Latif and Keenlyside, 2009), which may affect the overall BDC response ~~in the tropical Pacific often shows an El Niño Niño-like pattern~~ (Latif and Keenlyside, 2009). For example, ~~T~~ regional SST anomalies

associated with the El Niño Southern Oscillation (ENSO) have been shown to itself-affects the BDC both through modulation of the Northern Hemisphere (NH) winter stratospheric circulation (Manzini et al., 2006) and tropical lower stratospheric upwelling (Marsh and Garcia, 2007; Randel et al., 2009). Using CMAM, Simpson et al. (2011) attribute the increase in boreal winter tropical lower stratospheric upwelling under El Niño to increased resolved wave forcing in the Southern Hemisphere (SH) subtropical lower stratosphere, which was caused by altered wave sources in the troposphere under El Niño. In contrast, Calvo et al., (2010) using the Whole Atmosphere Community Climate Model (WACCM), attribute the increased tropical upwelling during El Niño to changes in the propagation and dissipation of parameterized gravity waves caused by the anomalous location and intensity of the subtropical jets ~~highlighting the model-specific nature of gravity wave drag parameterizations~~. (Garfinkel et al., (2013) showed that decadal trends comprising of warming in the Indian Ocean and the warm pool region can drive changes in tropical lower stratospheric upwelling. Therefore, while a uniform SST increase can generate most-much of the canonical pattern of long-term tropical upper tropospheric warming, through impacts on tropical convection and the water vapour and lapse rate feedbacks (e.g. Chen et al., 2013), the spatial pattern of SST trends may also affect the BDC. Lin et al. (2015) showed an approximately linear relationship between tropical annual mean surface temperature and anomalous lower stratospheric mass flux in the GFDL-CM3 model that held on interannual (i.e. ENSO), decadal and centennial timescales. However, on multi-decadal timescales this calculation aliases the direct atmospheric radiative effects of GHGs, the SST pattern effect and the SST magnitude into one term: ~~Hence, under climate change the direct radiative effect of CO<sub>2</sub> (rapid adjustment) (Olsen et al., 2007; Sigmond et al., 2004), as well as the magnitude and pattern of SST change may contribute to simulated changes in the BDC.~~

While previous literature suggests that the ~~three distinct radiative effects of GHGs, the SST magnitude and the SST pattern distinct effects~~ may contribute to projected changes in the BDC, no previous study has explicitly quantified their importance; this is the goal of our study. Here, we perform climate model experiments to decompose the response of the BDC to an abrupt quadrupling of CO<sub>2</sub> into three components: 1) the rapid adjustment, or direct component, associated with CO<sub>2</sub> radiative effects in the absence of SST change; 2) a contribution from the global-average sea surface temperature (SST) change termed throughout the rest of the study as a global uniform SST warming; and 3) the SST pattern effect. The goal is to understand the distinct contributions of the three components and assess the extent to which they can be combined to explain the overall BDC response. We further compare the magnitudes of the rapid adjustment and SST pattern effects on the BDC with the effect of spread in global mean warming SST change due to CO<sub>2</sub> across climate models. The remainder of the paper is laid out as follows: Section 2 describes the atmospheric model and experimental set-up; Section 3 presents the results and Section 4 summarises our main findings and conclusions.

## 2 Data and Methods

### 2.1 Atmospheric model description

125 We use the Hadley Centre Global Environment Model version 3 (HadGEM3) variant of the Met Office Unified Model (MetUM) version 8.4, which has been used for both numerical weather prediction and climate simulation. It is configured with the Global Atmosphere (GA4.0) and comprises a non-hydrostatic fully compressible dynamical core that uses a semi-implicit semi-Lagrangian advection scheme in terrain-following hybrid height coordinates (Walters et al., 2014). We run the atmosphere-only configuration (HadGEM3-A) at N96 horizontal resolution ( $1.875^\circ \times 1.25^\circ$ ,  $\sim 135$  km in mid-latitudes) with  
130 85 levels (L85) from the surface to an altitude of  $\sim 85$  km. Interactions of the flow blocking drag associated with the orographic gravity wave drag (OGWD) are parameterized, as detailed in Webster et al. (2003). Similarly, a spectral sub-grid parameterization is used for the representation of the gravity wave drag induced in the upper stratosphere and mesosphere, forced by non-orographic sources (NOGWD) such as convective processes and fronts, which enables HadGEM3 to simulate a realistic quasi-biennial oscillation (QBO) as detailed in Scaife et al. (2002).

### 135 2.2 Experiment design

Seven 50-year-long time-slice simulations were performed with HadGEM3-A with fixed boundary conditions including prescribed SSTs and sea ice. The experiment names and IDs are shown in Table 1. The reference simulation (run A) uses boundary conditions, including greenhouse gas (GHG) concentrations, natural and anthropogenic primary aerosol or reactive gas emissions, set to pre-industrial (year 1850) values following the Coupled Model Intercomparison Project 5 protocol  
140 (CMIP5; Lamarque et al., 2010; Taylor et al., 2012). The reference SSTs and sea ice concentrations (SIC) are annually repeating fields taken as the monthly-mean multi-model mean (MMM) from the CMIP5 piControl simulations (Taylor et al., 2012). The MMM reference SST and SIC fields are constructed from the average of the last 150 years of the piControl experiments from the 26 CMIP5 models listed in the [Supplementary material Information](#) (Table S1).

Six perturbation experiments are performed to isolate different components of the long-term response in the CMIP5 abrupt-  
145  $4\times\text{CO}_2$  experiment, which instantaneously quadruples  $\text{CO}_2$  from its preindustrial concentration. We first calculate the CMIP5 monthly-mean MMM SST in the abrupt- $4\times\text{CO}_2$  experiment using the final 50 years (years 101-150) of each model run (Table S1). The annual-mean SST anomalies compared to the reference preindustrial state are shown in Figure 1(a). Note that in all the perturbation experiments, SIC is held fixed at the reference values. This is artificial, but it enables the effects of SSTs on the BDC and associated mechanisms to be isolated from the possible effects of changing sea ice on the stratosphere, ~~which~~  
150 ~~has been proposed but is more uncertain~~ (e.g. Kim et al., 2014; McKenna et al., 2018). **We performed a separate experiment in which SIC was also changed to the CMIP5 MMM  $4\times\text{CO}_2$  response along with global SSTs and atmospheric  $\text{CO}_2$ , but this showed no significant effect of changing SIC on the BDC (not shown) and therefore will not be discussed further.**

The first perturbation experiment (run B) accounts for the full (atmosphere + SST) abrupt- $4\times\text{CO}_2$  response and is designed to simulate the long-term ~~centennial-quasi-equilibrium state in~~ response to ~~the abrupt-~~ $\text{CO}_2$  forcing. (Ceppi et al., (2018))The

155 second perturbation experiment (C) only accounts for the CO<sub>2</sub> rapid adjustment by quadrupling atmospheric CO<sub>2</sub> concentrations while holding SSTs and SIC at their preindustrial values. The third experiment (D) imposes a monthly-varying globally uniform SST anomaly derived from the global mean multi-model mean 4×CO<sub>2</sub> SST anomaly relative to the control. In the annual and multi-model mean this is equal to 3.4 K (Figure 1b). Note the CMIP5 MMM global SST anomaly is smaller than the global mean surface air temperature (GSAT) change in the abrupt-4×CO<sub>2</sub> experiment because land areas warm more  
160 than the ocean (e.g., (Joshi and Gregory, 2008)).— In the fourth perturbation experiment (E), we subtract the monthly-varying uniform warming value from the 4×CO<sub>2</sub> anomalies to impose the local deviations in SST from the global uniform value (i.e. the SST pattern). The SST pattern is shown in Figure 1(c); it is comprised of relatively stronger warming across the tropics in the Pacific, Atlantic and Indian Ocean basins and in the North Pacific, and relatively weaker warming across the Southern Ocean, in the North Pacific warming hole region and in the vicinity of the South Pacific stratocumulus decks.

165 By construction, the sum of the SSTs anomalies in runs D and E equals the full SST anomalies of run B. The annual mean SST anomalies associated with experiments B, D and E, respectively, are shown in Figure 1. Note that the change in annual-mean global surface air temperature (GSAT) simulated in runs B and D (4.3 K and 4.0 K, respectively) is larger than the imposed global mean SST anomaly, partly because of the enhanced warming response over land (4.3 K and 4.0 K, respectively). While SSTs are held fixed in run B, there are changes to land temperatures that cause a small GSAT response  
170 (0.43 K). Finally, although the global mean SST change in run D-E is zero by construction, there are changes to land temperatures that lead to a small GSAT response (0.45 K).

There is substantial inter-model spread in the modelled global mean SST change in the abrupt-4×CO<sub>2</sub> experiments (Flato et al., 2013). To investigate the effect of this spread on the BDC, and to place the rapid adjustment and SST pattern effects into the context of model uncertainty in the global mean surface warming due to CO<sub>2</sub>, we perform two further uniform SST warming  
175 sensitivity runs. These are chosen to be the lowest (annual-mean ~2.1 K; run F) and highest (annual-mean ~4.9 K; run G) global mean SST changes from the 26 CMIP5 models used in this study. These values come from the INMCM4 (Volodin, 2013) and IPSL-CM5A-LR (Dufresne et al., 2013) models, respectively. The annual-mean GSAT change in runs F and G is 3.0 and 6.1 K, respectively.

Since HadGEM3-A the model does not include interactive chemistry, we prescribe zonal-mean preindustrial ozone  
180 concentrations in all our 4×CO<sub>2</sub> perturbation runs following the Coupled Model Intercomparison Project 6 (CMIP6; Eyring et al., 2016) protocol, based on. In this case, for simplicity, we prescribe the zonal-mean ozone concentrations used in the CMIP6 experiments run with HadGEM3-GC3.1 (Kuhlbrodt et al., 2018; Williams et al., 2018). It should be noted that keeping O<sub>3</sub> ozone concentrations fixed in all our experiments will implicitly neglect the effects of any O<sub>3</sub>-ozone feedbacks from both the chemical effects of increased CO<sub>2</sub> and the transport effects from an altered BDC; this includes effects on the  
185 thermal structure of the upper troposphere especially around the tropical upper troposphere and lower stratosphere (Nowack et al., 2015; Chiodo and Polvani, 2017) and on upper stratospheric temperatures (Maycock, 2016).

### 2.3 Residual circulation diagnostics

To diagnose the BDC and its changes we make use of the Transformed Eulerian Mean circulation diagnostics (TEM; Andrews et al., 1987; Andrews and McIntyre, 1976, 1978) as calculated internally by the model. The TEM residual circulation velocities ( $\bar{v}^*$ ,  $\bar{w}^*$ ) are defined as (Andrews et al., (1987):

$$\bar{v}^* = \frac{1}{\rho_0 a \cos \phi} \frac{\partial \bar{\Psi}^*}{\partial z}, \quad \bar{w}^* = \frac{1}{\rho_0 a \cos \phi} \frac{\partial \bar{\Psi}^*}{\partial \phi}, \quad (1)$$

$$\bar{v}^* = \bar{v} - \frac{1}{\rho_0} \frac{\partial}{\partial z} \left[ \frac{\rho_0 \overline{v'\theta'}}{\partial \theta / \partial z} \right], \quad \bar{w}^* = \bar{w} + \frac{1}{a \cos \phi} \frac{\partial}{\partial \phi} \left[ \frac{\overline{v'\theta'} \cos \phi}{\partial \theta / \partial z} \right] \quad (1)$$

195

where overbars denote a zonal-mean quantity and primes the departure from the zonal-mean.  $v$  and  $w$  are the meridional and vertical components of wind velocity respectively,  $\rho_0$  is the log-pressure density,  $z = -H \ln(p/p_s)$  is the log-pressure vertical coordinate (height),  $H$  is the scale height,  $p$  is the pressure at a specified level with  $p_s$  the pressure at the surface,  $\overline{v'\theta'}$  is the eddy heat flux,  $\theta$  is the potential temperature,  $\alpha$  is the Earth radius and  $\phi$  is the latitude. and  $\bar{\Psi}^*(\phi, z)$  is the residual meridional mass streamfunction. Using  $\bar{v}^*$  from equation 1 we further calculate the residual mass streamfunction  $\bar{\Psi}^*(\phi, z)$  as:

200

$$\bar{\Psi}^*(\phi, z) = \frac{2\pi a \cos \phi}{g} \int_{\text{bottom}}^{\text{top}} \bar{v}^* dp, \quad (2)$$

where  $g$  is the acceleration due to gravity. Equation 2 is integrated from the top of atmosphere to the surface using the boundary condition that  $\bar{\Psi}^* = 0$  at the top of the atmosphere ( $p=0$ ). Subsequently, we calculate the net downward mass flux in each hemisphere, by finding  $\bar{\Psi}^*_{max}$  and  $\bar{\Psi}^*_{min}$  in the NH and SH, respectively, at each pressure level. The net tropical upward mass flux, which is equal to the sum of the downward mass fluxes in each hemisphere, can then be expressed as (Rosenlof, 1995):

205

$$\text{Tropical upward mass flux} = 2\pi a (\bar{\Psi}^*_{max} - \bar{\Psi}^*_{min}). \quad (3)$$

We apply the “downward control” principle (DCP; Haynes et al., 1991) to further separate the contributions to the tropical upward mass flux from resolved waves due to the divergence of Eliassen-Palm flux (EPF) and contributions from OGWD and NOGWD. Resolved waves and parameterized gravity wave drag (OGWD/NOGWD) constitute the eddy-induced total zonal forces  $\bar{F}$ . Under steady-state conditions, the  $\bar{\Psi}^*(\phi, z)$  at a specified log(pressure)-height,  $z$ , is related to the vertically-integrated  $\bar{F}$  above that level along a surface of constant zonal-mean absolute angular momentum  $\bar{m} = a \cos \phi (\bar{v} + a \Omega \cos \phi)$ , where  $\bar{v}$  is the

210

zonal-mean zonal wind and  $\Omega$  is Earth's rotation rate (Haynes et al., 1991). Outside of the tropics,  $\bar{m}$  is approximately constant  
 215 at a fixed latitude,  $\phi$ , resulting in the following equation (Haynes et al., 1991):

$$\bar{\Psi}^*(\phi, z) = \int_z^\infty \left\{ \frac{\rho_0 \alpha^2 \bar{F} \cos^2 \phi}{\bar{m}_\phi} \right\}_{\phi=\phi(z)} dz, \quad (4)$$

where  $\bar{m}_\phi \approx -2\Omega\alpha^2 \sin\phi \cos\phi$  is the quasi-geostrophic limit. The boundary conditions are  $\bar{\Psi}^* \rightarrow 0$  and  $\rho_0 \bar{w}^* \rightarrow 0$  as  $z \rightarrow \infty$ .

## 220 3 Results

### 3.1 Zonal-mean temperature response

Figure 2 shows latitude-pressure cross-sections of the annual-mean and zonal-mean temperature anomalies from the reference preindustrial simulation for perturbation runs B, C, D and E. The full response (Fig. 2a) exhibits the canonical pattern of temperature change due to increased CO<sub>2</sub>, with tropospheric warming that is maximum in the tropical upper  
 225 troposphere (by ~8 K) and stratospheric cooling that increases with height (Collins et al., 2013). Note that Arctic amplification in the lower troposphere is small here compared to coupled atmosphere-ocean models (Collins et al., 2013), presumably because we do not impose sea ice changes in the runs.

The rapid adjustment due to changes in atmospheric CO<sub>2</sub> (Fig. 2b) accounts for most of the stratospheric cooling seen in the full response, with cooling of ~15 K in the upper stratosphere. However, the stratospheric cooling in run C (Fig. 2b) is  
 230 more uniform in latitude than in the full experiment, and more closely resembles the purely radiative response to CO<sub>2</sub> (Fels et al., 1980). In the troposphere, the rapid adjustment induces a weak (<1 K) warming that is fairly homogeneous and comes partly from the small changes in GSAT, since land temperatures are not held fixed. This weak tropospheric warming comes from heating of the land surface and changes to atmospheric absorption and emission of longwave radiation due to increased CO<sub>2</sub> concentrations. Most of the tropospheric zonal-mean warming is reproduced by imposing the uniform SST warming (Fig.  
 235 2c), including the tropical upper tropospheric amplification of up to 9 K and the extension of warming into the subtropical lower stratosphere in both hemispheres. In the stratosphere, the uniform SST warming induces an anomalous meridional temperature gradient, with cooling of 2-3 K in the tropical middle and upper stratosphere and warming in the extratropics and polar regions. This pattern accounts for most of the latitudinal variation in stratospheric cooling seen in the full response (Fig. 2a).

240 The SST pattern experiment (Fig. 2d) exhibits a similar morphology in the temperature response to the uniform SST warming run, albeit much weaker in amplitude. In the troposphere, the SST pattern induces a weak warming that is comparable in magnitude to the rapid adjustment (Fig. 2b), but with a weak upper tropospheric amplification that enhances the effect of

the uniform warming (Fig. 2c). This upper tropospheric amplification suggests enhanced tropical deep convection, which may be consistent with the imposed anomalous tropical SST warming (Fig. 1c).

245 The thick yellow lines in Figure 2 denote the tropopause pressure for each perturbation experiment. These can be compared to the climatological tropopause in the reference simulation (thick black lines). The lifting of the tropopause by ~1 km within the deep tropics in the full experiment comes mainly from the uniform SST warming (~80%) with the remaining 20% coming from the SST pattern. However, the maximum tropopause lifting (> 1.2 km) occurs in the extratropics of both hemispheres, especially over the Arctic polar cap (not shown).

### 250 3.2 Zonal-mean zonal wind response

The annual-mean zonal-mean zonal wind anomalies in the four perturbation experiments are shown in Figure 3. The full 4xCO<sub>2</sub> response (Fig. 3a) shows the familiar pattern of a strengthening and upward shift of the subtropical jets, a strengthening and poleward shift of the midlatitude westerlies in the SH, and increased westerlies in the SH stratosphere (Collins et al., 2013). The strengthened subtropical jets arise mainly from the uniform SST warming (Fig. 3c) with a small contribution from the SST pattern (Fig. 3d). In contrast, the rapid adjustment (Fig. 3b) does not induce a strengthening of the subtropical jets, but it does explain a significant part of the increased westerlies in the SH extratropics, particularly in the upper stratosphere. The SST pattern effect also contributes to the increased SH stratospheric westerlies, but the uniform SST warming shows the largest increase. In the NH, the full experiment shows stronger westerlies in the lower stratosphere and weakened westerlies near the subtropical stratopause. The anomalous lower stratospheric westerlies are contributed by the uniform warming in the 255 subtropics and midlatitudes and the rapid adjustment in the extratropics and polar region. The uniform warming also causes weakened westerlies in the subtropical upper stratosphere, with a smaller effect from the rapid adjustment.

The full 4xCO<sub>2</sub> response shows significant zonal wind anomalies in the tropical stratosphere between 50-1 hPa, which is also seen in the uniform SST warming experiment. [Investigation of the QBO characteristics in the experiments reveals changes in the period, magnitude and vertical penetration of the easterly and westerly QBO phases \(not shown\).](#) This is likely related 265 to changes to the QBO properties under climate change, which have been noted in other idealised GCM experiments (e.g. Kawatani et al., 2011), though a detailed investigation of the QBO is beyond the scope of this study.

The zero wind lines ( $\bar{u} = 0$ ), which demarcate the “critical lines” for linear stationary Rossby waves (Dickinson, 1968), are shown by the thick lines in Figure 3. In the stratosphere, there is a clear equatorward contraction of the zero wind lines in both hemispheres in the full 4xCO<sub>2</sub> experiment. Previous studies have connected this to increased penetration of Rossby wave 270 activity into the subtropical lower stratosphere (Shepherd and McLandress, 2011). The contraction of the zero wind lines is primarily due to the uniform SST warming, with a modest contraction also seen in the rapid adjustment and SST pattern experiments.

### 3.3 Residual circulation response

Figure 4 shows latitude-pressure cross-sections of the annual-mean residual vertical velocity ( $\bar{w}^*$ ) anomalies with respect to the reference simulation for experiments B, C, D and E. The uniform SST warming accounts for most of the increased tropical lower stratospheric upwelling (~70% between 30°-S and 30°-N over the layer 100 – 50 hPa) seen in the full 4×CO<sub>2</sub> response. However, there are also significant, but small, increases in tropical lower stratospheric upwelling induced by the rapid adjustment (~17%) and the SST pattern perturbations (~13%) (Fig. 4b, 4d). While comparatively small compared to the effect of the uniform SST warming, the increases in  $\bar{w}^*$  in the tropical lower stratosphere from the SST pattern are broadly comparable in magnitude to the effects of ENSO on tropical upwelling-like SST perturbations found in other modelling studies (Calvo et al., 2010; Simpson et al., 2011).

The boundaries where the residual vertical velocity changes sign from positive to negative, known as the turnaround latitudes (TL), are overlaid as thick lines in Figure 4. A quadrupling of CO<sub>2</sub> leads to a narrowing of the upwelling region between in the lower and middle stratosphere (shallow branch) that maximises around ~30 hPa (Hardiman et al., (2014). This arises predominantly from the uniform SST warming (Fig. 4c), with additional weaker contributions from the rapid adjustment and SST patterns (Fig. 4b and 4d). In contrast, in the deep branch of the BDC upper stratosphere (10 hPa) the upwelling region widens particularly in the NH (cf. (Hardiman et al., (2014). The widening of the upwelling region in the NH upper stratosphere arises almost entirely from the rapid adjustment, while the smaller tropical widening in the SH upper stratosphere is contributed by all three components.

We move now to evaluating the changes in downwelling in the extratropics. The full 4×CO<sub>2</sub> experiment shows enhanced downwelling over the Arctic throughout the stratosphere. Both the rapid adjustment and uniform SST warming induce comparable increases in downwelling in the Arctic, while the SST patterns do not produce significant  $\bar{w}^*$  changes in this region. In the SH, the full perturbation generates stronger downwelling in the upper stratosphere and weaker downwelling in the middle and lower stratosphere ( $p > 10$  hPa) below 10 hPa. All three components produce increased downwelling in the Antarctic upper stratosphere, with the largest change from the uniform SST warming and the rapid adjustment. In the lower stratosphere, the uniform SST and SST patterns both generate reduced downwelling as seen in the full 4×CO<sub>2</sub> experiment.

The relationship of the changes in residual circulation to the overall mass transport in the stratosphere can be seen in Figures 5 and 6, which shows the residual mass streamfunction anomalies ( $\Psi^*$ ) in the solstice seasons December-February (DJF) and June-August (JJA) in the four experiments. For comparison, Supplementary Information (Figure S1) shows the annual-mean  $\Psi^*$  responses. As the winter hemisphere cell is the dominant one, the climatological circulation in DJF and JJA is significantly stronger in the NH and SH, respectively. The largest response in both hemispheres occurs in DJF (Figure 5), while the NH exhibits a stronger response compared to the SH. In DJF, the response to the SST patterns in the NH is confined to the subtropical lower stratosphere (Fig 5d), while the rapid adjustment (Fig. 5b) and uniform SST warming (Fig. 5c) induce increased poleward transport across most of the stratosphere, with the latter showing around three times larger anomalies near the maximum in the subtropical lower stratosphere. The peak NH anomaly due to the rapid adjustment is around double that

for the SST patterns in DJF. Specifically, in the lower stratosphere (100 – 50 hPa) between 0° – 60°-N, the uniform SST warming accounts for ~65% of the full response, the rapid adjustment contributes ~26% and the SST patterns contribute the remainder. Conversely, in the middle and upper stratosphere between 30–1 hPa, over the same latitude bands, the rapid adjustment effect becomes more important, surpassing the contribution of the uniform SST warming accounting for the 48% and 46% of the full response, respectively. In JJA (Figure 6), the increase in the SH mass transport is largely present in the subtropics while the opposing changes in the mid-latitude lower stratosphere seen as a reduction in the streamfunction, arise from both the uniform SST warming (Fig. 6c) and the SST patterns (Fig. 6d). In the SH subtropical (0° – 30° S) lower stratosphere (100 – 50 hPa), the uniform SST warming ~~anomalies~~ accounts for ~70% of the full response with the rapid adjustment contributing roughly 20% ~~with~~ and the remaining 10% due to the SST patterns. The strengthened SH poleward transport due to the uniform SST warming is confined to the SH subtropical lower stratosphere, while the rapid adjustment (Fig. 6b) induces poleward flow that also extends into the NH and is associated with the deep branch of the BDC. However, it should be noted that the SH response is generally weaker than in the NH, especially in the middle and upper stratosphere over both solstice seasons. The deep branch of the circulation exhibits distinct hemispheric asymmetries explaining the differences in the magnitude of downwelling over the SH and NH polar caps seen in Figure 4. This asymmetry is associated with a significantly stronger poleward NH branch of the circulation compared to its SH counterpart with important contributions by an equally stronger NH mesospheric cell overall (not shown).~~The relationship of the changes in residual circulation to the overall mass transport in the stratosphere can be seen in Figure 5, which shows the annual mean residual streamfunction anomalies ( $\Psi^*$ ) in the four experiments. The full 4xCO<sub>2</sub> experiment shows enhanced poleward mass transport in both hemispheres (Hardiman et al., 2014) (Fig. 5a), with all three components of the total forcing contributing to this pattern albeit with different magnitudes. The positive streamfunction anomalies maximise in the NH lower stratosphere where the uniform SST warming (Fig. 5c) accounts for the majority of the full response, with the rapid adjustment being the next largest contributor (Fig. 5b) and lastly the SST patterns generating a small increase in poleward transport (Fig. 5d). In contrast, in the NH extratropical middle and upper stratosphere, all components contribute similarly to the enhanced poleward mass transport. In the SH, the uniform SST warming (Fig. 5c) and to a lesser extent the SST pattern experiment (Fig. 5d), induce an acceleration of the BDC in the lower stratosphere with the latter exhibiting a response that is confined to the subtropics. Over the Antarctic polar cap in the lower and middle stratosphere, there is no statistically significant response of the annual mean mass streamfunction in any of the perturbation experiments. As the winter hemisphere cell of the residual circulation is the dominant one (Rosenlof, 1995), the residual mass streamfunction anomalies in the solstice seasons December–February (DJF) and June–August (JJA) are shown in the supplementary material (Figures S1 and S2, respectively). These reveal broadly similar patterns to the annual mean in both seasons. The largest response in both hemispheres occurs in DJF, while the NH exhibits a stronger response compared to the SH. In DJF, the response to the SST patterns in the NH is confined to the subtropical lower stratosphere, while the rapid adjustment and uniform SST warming induce increase poleward transport across most of the stratosphere, with the latter showing around three times larger anomalies near the maximum in the subtropical lower stratosphere. The peak NH anomaly due to the rapid adjustment is around double that for the SST patterns in DJF. In JJA, the~~

340 ~~increase in the SH mass transport is largely present in the subtropics while in the extratropics there is a reduction in the streamfunction which comes from both the uniform SST warming and the SST patterns. The strengthened SH poleward transport due to the uniform warming is confined to the SH subtropical lower stratosphere, while the rapid adjustment induces poleward flow that also extends into the NH that is associated with the deep branch of the BDC.~~

~~An important question is~~ We lastly consider the extent to which the combined residual circulation anomalies from the rapid adjustment, global uniform SST, and SST pattern experiments match the full  $4\times\text{CO}_2$  response. This comparison is shown in ~~the sSupplementary Information~~ element (-Figure ~~S3S2~~). The main differences are that the combined responses overpredict the enhanced poleward flow in the NH extratropical lower stratosphere, while there are dipole anomalies straddling the equator in the tropical mid-stratosphere associated with the differences seen in the QBO features across the experiments. Nevertheless, the differences between the linear sum of responses and the full experiment are generally small compared to the overall changes, which supports the use of the experiments to decompose the total response into separate parts.

### 3.4 Wave forcing and downward control

To understand the changes in residual circulation shown in Figures 4-6 ~~and~~, we now focus on the wave forcing in each experiment. As the distribution of wave forcing shows a strong annual cycle, we separate the changes into the winter and summer seasons in each hemisphere (DJF and JJA) ~~as in Figures 5 and 6~~. Figure ~~6-7~~ shows the DJF average Eliassen–Palm flux divergence (EPFD) anomalies from preindustrial for runs B, C, D and E along with the anomalous ~~Eliassen–Palm flux~~ EPF vectors. ~~For that matter, w~~ We multiply the EPFD anomalies with  $\cos\phi$  ~~as it represents~~ the torque exerted on the zonal flow ~~coinciding with the patterns of the associated residual circulation anomalies shown in section 3.3~~. The full experiment (Fig. ~~6a7a~~) shows increased EPF divergence in the NH extratropical upper stratosphere and in the midlatitude middle stratosphere. In the SH, there is a broad region of enhanced EPF convergence peaking around  $50^\circ$ – $60^\circ$  S over a layer spanning 3 to 70 hPa. There is a reduction in EPF convergence near the SH subtropical stratopause. Between  $\sim 50^\circ$ – $70$  hPa, there is enhanced EPF convergence in the tropics and subtropics in both hemispheres. This modulation in the location of the maximum in the resolved wave forcing is associated with the equatorward movement of the critical layers (Fig. 3), allowing more Rossby wave activity to penetrate into the subtropical latitudes, accelerating the shallow branch of the BDC, consistent with the findings of Shepherd and McLandress (2011).

365 The rapid adjustment and uniform SST warming contribute similar increases in EPF convergence in the NH upper stratosphere in DJF (Figs. ~~6b-7b~~ and ~~6e7c~~). In the NH middle stratosphere, the uniform SST warming explains most of the increase in EPF convergence seen in the full experiment, but the rapid adjustment does contribute in the region  $20^\circ$ – $40^\circ$  N. The uniform SST warming also contributes to most of the increase in EPF convergence in the lower to middle SH extratropical stratosphere in austral summer, but the rapid adjustment and SST pattern (Fig. ~~6d7d~~) do make smaller but significant contributions to the increased wave forcing in that region. The uniform SST warming produces most of the enhanced EPF convergence in the tropical and subtropical upper troposphere-lower stratosphere (UTLS).

Figure 7-8 shows the EPFD anomalies in JJA in each experiment. The picture in the summer NH in the full experiment is similar to that in the SH in DJF (Fig. 6a7a). Specifically, there is anomalous EPF divergence in the extratropical lower stratosphere and anomalous EPF convergence in the middle to upper stratosphere, representing an upward shift and extension of the region of climatological EPF convergence in this region (contours). Near the subtropical stratopause there is anomalous EPF divergence that comes mainly from the rapid adjustment (Fig. 7b8b). The anomalous EPF convergence in the middle stratosphere comes mainly from the uniform SST warming (Fig. 7c8c) with smaller but significant contributions from the rapid adjustment and SST patterns (Fig. 7d8d). In the winter SH, the picture is rather different from the NH in DJF. The full experiment shows anomalous EPF divergence in the SH upper stratosphere, which represents a weakening of the climatological EPF convergence in this region (contours). This is attributed mainly to the uniform SST warming, but there are also significant EPF convergence anomalies near the SH subtropical stratopause from both the rapid adjustment as well as the SST patterns. The changes in EPFD in the SH middle and lower stratosphere in austral winter have a more complex structure. The full experiment shows a tripolar pattern between 30 to 70 hPa, with anomalous EPF convergence poleward of 60° S and between 20°–40° S and anomalous divergence between 40°–60° S. This pattern is mainly reproduced in the uniform SST warming experiment but with a smaller contribution to the two regions of anomalous EPF convergence from the rapid adjustment. Previous studies have demonstrated mechanisms for tropospheric warming to influence the stratospheric EPFD and residual circulation (e.g., Shepherd and McLandress, 2011), but the mechanism through which the rapid adjustment acts on EPFD in the upper stratosphere is less well understood. The radiative cooling in the stratosphere due to increased CO<sub>2</sub> is relatively uniform in latitude (Fels et al., 1980), so we do not expect large direct changes in zonal wind through thermal wind balance. However, the temperature response to CO<sub>2</sub> represents a weakening of the vertical temperature gradient, particularly in the upper stratosphere where the cooling is larger. The characteristics for wave propagation and refraction can be quantified using a measure of refractive index (e.g., Matsuno, 1970) that is dependent on the Brunt-Väisälä frequency ( $N^2 = g/\theta(d\theta/dz)$ ). Hence, we hypothesise that the changes in background temperature structure due to the CO<sub>2</sub> radiative effects alter the propagation of Rossby waves, particularly in the upper stratosphere, and this leads to the changes in EPFD shown in Figures 7 and 8.

The ~~total~~ anomalous residual circulation is driven by both resolved and parameterized wave forcing. The seasonal parameterized wave forcing (NOGWD and OGWD) anomalies are shown in the ~~supplementary~~ Supplementary material Information (Figures S34-S45 for DJF and Figures S56-S67 for JJA). The peak changes in parameterized wave forcing are smaller than the anomalous resolved wave forcing by around a factor of two. The anomalous NOGWD is mainly in the upper stratosphere and comes from the uniform SST warming. There is anomalous OGWD (Figs. S45 and S67) in the winter hemispheres near the edge of the polar vortex, which has comparable contributions from the rapid adjustment and the uniform SST warming.

We now quantify the contributions of the different wave types to the anomalous mass circulation in the ~~shallow and deep branches of the BDC~~ lower and upper stratosphere. Figures 8-9 and 109 show latitudinal profiles of the annual-mean mass streamfunction anomalies in each experiment at 70 hPa and 10 hPa, respectively, along with the DCP inferred contributions

405 from the resolved and parameterized components of the wave forcing. The DCP calculation for the total wave forcing underestimates the directly calculated maximum streamfunction anomaly in the model by around 20%.

In the lower stratosphere at 70 hPa, the estimated streamfunction anomalies from the total wave forcing in the full 4×CO<sub>2</sub> experiment come mainly (>80%) from the resolved wave forcing (Fig. 8a9a), with a smaller and more homogeneous contribution from the parameterized wave drag. The resolved wave forcing explains almost all of the DCP estimated response in the rapid adjustment experiment (Fig. 8b9b) and most of it in the uniform SST warming (Fig. 8c9c) case. The component that contributes the smallest increase in streamfunction at 70 hPa, the SST pattern experiment (Fig. 8d), shows roughly equal contributions from parameterized and resolved wave forcing. The overall dominance of the resolved wave forcing for the strengthened ~~shallow branch~~ BDC in the lower stratosphere is consistent with the larger changes in resolved wave drag in this region in the lower and middle stratosphere (Figures 6-7 and 78) compared to the parameterized wave forcing changes in this region (Figures S4S3-S7S6).

In the ~~deep branch in the~~ upper stratosphere (10 hPa), the full 4×CO<sub>2</sub> experiment shows contributions to the enhanced streamfunction from both resolved and parameterized wave forcing (Fig. 9a10a). In the NH, the EPFD contribution explains around two thirds of the total DCP estimated streamfunction anomalies and GWD around one third. The positive NH streamfunction anomaly from EPFD poleward of 30°N comes from both the rapid adjustment (Fig. 9b10b) and the uniform SST warming (Fig. 9c10c). In contrast, the positive streamfunction anomaly in the ~~deep branch~~ upper stratosphere from parameterized wave drag comes mainly from the uniform SST warming (Fig. 9e10c).

In the SH, the picture in the Full experiment is somewhat more complex, with the major contribution to the enhanced poleward mass transport coming from GWD, which is partly offset by an opposite contribution from the EPFD. This positive SH streamfunction anomaly associated with EPFD comes mainly from the uniform SST warming (Fig. 9e10c), which also generates enhanced SH poleward transport via enhanced GWD. This increased poleward flow in the SH ~~deep branch~~ upper stratosphere is further increased by the rapid adjustment (Fig. 9b10b) with contributions from both resolved and parameterized wave drag. In both hemispheres, the SST pattern has little effect on the wave forcing ~~of the deep branch in the upper stratosphere~~ (Fig. 9d10d).

### 3.5 Uncertainty in global mean SST response

430 Figure 10-11 summarizes the results by showing the annual-mean tropical upward mass flux anomalies in the different experiments in the shallow and the deep branch of the BDC, at 70 hPa (Fig. 10a11a) and 10 hPa (Fig. 10b11b), respectively. Also shown are the mass flux anomalies from the high and low uniform warming experiments (runs F and G), which span the spread in 4×CO<sub>2</sub> global mean SST response across the CMIP5 models. In the lower branch of the BDC, the annual-mean tropical upward mass flux increases by 45% in the full experiment compared to piControl ( $3.1 \times 10^9$  kg s<sup>-1</sup>). The uniform SST warming accounts for ~70% of this increase, with the rapid adjustment (~20%) and SST patterns (~10%) contributing the remainder in comparable amounts. The central estimates of the mass flux anomalies at 70 hPa in the three uniform SST warming (2.1, 3.4, 4.9 K) experiments are 1.4, 2.3 and  $3.4 \times 10^9$  kg s<sup>-1</sup>, which gives an approximate linear scaling of  $0.7 \times 10^9$

kg s<sup>-1</sup> K<sup>-1</sup> (~10% K<sup>-1</sup>). In the ~~shallow branch of the BDC~~ lower stratosphere, the uncertainty from the CMIP5 model spread in global mean SST response to 4×CO<sub>2</sub> is larger than the contribution from the rapid adjustment and the SST pattern effect.

440 In the ~~deep branch~~ upper stratosphere at 10 hPa, the total mass flux increases by around 35% in the full experiment ( $0.6 \times 10^9$  kg s<sup>-1</sup>). This increase comes almost equally from the rapid adjustment (~ 40%) and the uniform SST warming (~ 45%), with the remaining ~ 15% contribution coming from the SST pattern effect, **though the latter is not statistically distinguishable from internal variability**. The central estimates of mass flux anomalies at 10 hPa in the three uniform SST warming experiments are 0.17, 0.29 and  $0.50 \times 10^9$  kg s<sup>-1</sup>, which gives an approximate linear scaling with global mean SST of  $0.11 \times 10^9$  kg s<sup>-1</sup> K<sup>-1</sup>  
445 (~ 7% K<sup>-1</sup>). In the ~~deep branch~~ upper stratosphere, the magnitude of the anomalous mass flux due to the rapid adjustment is therefore comparable to the uncertainty from the model spread in global mean SST response to 4×CO<sub>2</sub>.

#### 4 Discussion and conclusions

We have performed idealised experiments with the HadGEM3-A model to decompose the long-term Brewer-Dobson circulation response to an abrupt quadrupling in CO<sub>2</sub> into three components: 1) a rapid atmospheric adjustment where CO<sub>2</sub> is added to the atmosphere but sea surface temperatures (SST) are held fixed; 2) a contribution from the global-average SST  
450 change; and 3) an SST pattern effect. The SST anomalies in response to the abrupt 4×CO<sub>2</sub> perturbation were derived from the CMIP5 multi-model ensemble. The multi-model annual–mean global-mean SST anomaly over the final 50 years of the CMIP5 abrupt-4×CO<sub>2</sub> runs is 3.4 K. The SST pattern (i.e. the local deviation from the global mean value) shows relatively **warmer-higher** SST across the tropical oceans and most of the Northern hemisphere and relatively cooler SST across much of  
455 the Southern Ocean and in the northern North Atlantic. The HadGEM3-A simulations are perturbed from a reference preindustrial state, and sea ice concentrations are held fixed to enable a clean separation of the effects of SST without combining this with the potential effect of sea ice changes on the stratosphere (e.g., Kim et al., 2014).

In the tropical lower stratosphere, the 45% increase in the annual–mean mass transport by the BDC under the full 4×CO<sub>2</sub> perturbation comes mainly (~70%) from the uniform SST warming **consistent with the findings of** (Lin et al., (2015). The remainder comes from the rapid adjustment (~20%) and the SST pattern effect (~10%). The amplitude of the SST pattern effect on the mass transport in the ~~shallow branch~~ lower stratosphere is broadly comparable to that found on interannual timescales associated with ENSO (Calvo et al., 2010; Simpson et al., 2011), though note that **while** the SST pattern imposed here **shows enhanced warming in the equatorial Pacific, by construction it contains global structure; including relative warming across the tropical oceans and North Pacific and relative cooling in the Southern Ocean (Fig. 1c)**. In the upper stratosphere,  
465 where the deep branch of the BDC occurs, the increase in the BDC mass transport under abrupt-4×CO<sub>2</sub> comes from the rapid adjustment and the uniform SST warming in roughly equal measure. The results are consistent with studies that show an important role for the strengthening of the subtropical jets under climate change (e.g., Garcia and Randel, 2008; Lin and Fu, 2013; McLandress and Shepherd, 2009; Shepherd and McLandress, 2011), which in the decomposition performed here comes mainly from the uniform SST warming. However, our ~~results~~ also demonstrate **that an increase of the BDC in the upper**

470 stratosphere comes mainly ~~an important role for~~ from the radiative cooling of the stratosphere by CO<sub>2</sub>, ~~which in the~~  
~~decomposition performed here comes mainly in~~ as seen in the rapid adjustment component of the response, ~~for driving the~~  
~~increase in the deep branch of the BDC~~. This means that in transient atmosphere-ocean abrupt-4×CO<sub>2</sub> experiments, there are  
475 expected to be different characteristic timescales for the BDC response. In the lower stratosphere, the timescale of the BDC  
response will be mainly determined by the rate of tropospheric warming and associated changes to upper tropospheric heating  
and subtropical jet strength, while in the upper stratosphere there will be a fast timescale associated with the CO<sub>2</sub> radiative  
cooling and a slow timescale also tied to the tropospheric warming. The results therefore demonstrate the existence of two  
timescales in the response of the BDC to increasing CO<sub>2</sub>, with the relative importance of each timescale for the long-term  
response being height dependent.

We further examined the effect of the uncertainty in global mean SST response to increased CO<sub>2</sub>, as a proxy for model  
480 spread in equilibrium climate sensitivity. The range in the global mean SST response across the CMIP5 models is 2.1 to 4.9  
K. Further experiments imposing these global uniform SST values show an increase in the ~~shallow branch~~ lower stratosphere  
(70 hPa) upward mass flux of  $1.4 \times 10^9$  and  $3.4 \times 10^9$  kg s<sup>-1</sup>, respectively, which can be compared to the increase of  $2.3 \times 10^9$   
kg s<sup>-1</sup> in the multi-model mean global SST experiment. In the ~~deep branch~~ upper stratosphere (10 hPa), the upward mass flux  
change for uniform SST warming of 2.1 and 4.9 K is  $0.17 \times 10^9$  and  $0.5 \times 10^9$  kg s<sup>-1</sup>, respectively, which can be compared to  
485  $0.29 \times 10^9$  kg s<sup>-1</sup> in the multi-model mean global SST experiment. Therefore, in the lower stratosphere the contribution from  
the uniform SST warming and its uncertainty is larger than the rapid adjustment and SST pattern effects on the ~~BDC in the~~  
~~lower stratosphere~~ ~~shallow branch of the BDC~~. However, in the upper stratosphere (10 hPa) the uncertainty in the magnitude  
of global mean SST increase across models is comparable to the magnitude of the rapid adjustment effect on the ~~increased~~  
~~deep branch of the BDC~~.

490 Using the tropical mass flux anomalies described above and the GSAT changes in the experiments given in Section 2.2,  
we calculate a linear dependence of the tropical upward mass flux on GSAT of  $0.62 \times 10^9$  kg s<sup>-1</sup> K<sup>-1</sup> (~9% K<sup>-1</sup>) at 70 hPa and  
 $0.10 \times 10^9$  kg s<sup>-1</sup> K<sup>-1</sup> (~6% K<sup>-1</sup>) at 10 hPa. Hardiman et al. (2014) examined CMIP5 models and calculated a multi-model mean  
trend in 70 hPa upward mass flux of 3.2% decade<sup>-1</sup> over 2006-2099 in the Representative Concentration Pathway 8.5 (RCP8.5)  
emissions scenario. The multi-model mean change in GSAT between 2081-2100 relative to 1986-2005 is 3.7 K in the RCP8.5  
495 scenario (Collins et al., 2013). This gives an approximate multi-model mean GSAT trend for the 21<sup>st</sup> century of 0.35 K decade<sup>-1</sup>.  
Dividing these two numbers gives an estimate for the relationship between 70 hPa mass flux and GSAT of ~9% K<sup>-1</sup>. This is  
in ~~relatively good~~ ~~almost exact~~ agreement with our results, despite the different modelling approaches, though our estimate  
would be slightly larger if the contributions from the rapid adjustment and SST pattern effects, which are implicitly included  
in the simulations used by Hardiman et al. (2014), were accounted for. The comparison is further complicated by the  
500 projected ~~ion~~ reduction in the BDC due to ozone recovery (e.g., Oman et al., 2009), which offsets part of the GHG-driven  
increase over the 21<sup>st</sup> century; this effect is also included in the 21<sup>st</sup> century scenario simulations used by Hardiman et al.  
(2014) and, if removed, this would presumably make the inferred relationship to GSAT larger than the ~9% K<sup>-1</sup> estimated  
above based on the CMIP5 RCP8.5 scenario.

The CO<sub>2</sub> perturbation applied here is large compared to projected CO<sub>2</sub> concentrations during the 21<sup>st</sup> century based on  
505 current mitigation commitments under the United Nations Framework Convention on Climate Change (UNFCCC) 2015 Paris  
Agreement. For a smaller increase in CO<sub>2</sub>, the rapid adjustment and uniform SST warming contributions are expected to be  
smaller; in this case the SST pattern effect would become proportionately more important. Our experiments have neglected  
any feedbacks that induce stratospheric ozone changes; it has been shown that the ozone response to 4×CO<sub>2</sub> affects the zonal-  
mean extratropical circulation (Chiodo and Polvani, 2017); it would be interesting to also examine the effects of ozone on the  
510 BDC in the future. The experiments are designed to study the long-term centennial response to an abrupt quadrupling of CO<sub>2</sub>,  
and they have only been performed with one model. The model contains mean state biases that could affect some of the details  
of the responses described here. Studies with other coupled atmosphere-ocean models ~~that could be used and those that~~  
examine the transient response of the BDC to CO<sub>2</sub> would therefore be insightful.

#### *Data Availability*

515 All model output is available from the authors upon request.

#### *Author Contributions*

ACM and AC designed the study. AC ran the model simulations and analysed the data. AC and ACM interpreted the data and  
wrote the article with input from MPC.

#### *Competing interests*

520 The authors declare no competing interests.

#### *Acknowledgments*

AC was supported by a University of Leeds Anniversary Postgraduate Scholarship. ACM was supported by a NERC  
Independent Research Fellowship grant NE/M018199/1 and the European Union's Horizon 2020 Research and Innovation  
Programme under grant agreement No. 820829 (CONSTRAIN project). MPC acknowledges support through the NERC  
525 SISLAC grant NE/R001782/1. The model simulations were performed on the NERC ARCHER HPC facility. We acknowledge  
the World Climate Research Programme's Working Group on Coupled Modelling, which is responsible for CMIP, and we  
thank the climate modelling groups (listed in Table S1 of this paper) for producing and making available their model  
output. The analysis and visualization of the study were performed using the NCAR Command Language (NCL).

## References

- 530 Andrews, D. G. and McIntyre, M. E.: An exact theory of nonlinear waves on a Lagrangian-mean flow, *Journal of Fluid Mechanics*, 89(4), 609–646, doi:10.1017/S0022112078002773, 1978.
- Andrews, D. G. and McIntyre, M. E.: Planetary Waves in Horizontal and Vertical Shear: The Generalized Eliassen-Palm Relation and the Mean Zonal Acceleration, *Journal of the Atmospheric Sciences*, 33(11), 2031–2048, doi:10.1175/1520-0469(1976)033<2031:PWIHAV>2.0.CO;2, 1976.
- 535 Andrews, D. G., Holton, J. R. and Leovy, C. B.: *Middle Atmosphere Dynamics*, International Geophysical Series, Vol. 40, 1987.
- Banerjee, A., Maycock, A. C., Archibald, A. T., Abraham, N. L., Telford, P., Braesicke, P. and Pyle, J. A.: Drivers of changes in stratospheric and tropospheric ozone between year 2000 and 2100, *Atmospheric Chemistry and Physics*, 16(5), 2727–2746, doi:10.5194/acp-16-2727-2016, 2016.
- 540 Birner, T. and Bönisch, H.: Residual circulation trajectories and transit times into the extratropical lowermost stratosphere, *Atmospheric Chemistry and Physics*, 11(2), 817–827, doi:10.5194/acp-11-817-2011, 2011.
- Brewer, A. W.: Evidence for a world circulation provided by the measurements of helium and water vapour distribution in the stratosphere, *Quarterly Journal of the Royal Meteorological Society*, 75(326), 351–363, doi:10.1002/qj.49707532603, 1949.
- 545 Butchart, N. and Scaife, A. A.: Removal of chlorofluorocarbons by increased mass exchange between the stratosphere and troposphere in a changing climate, *Nature*, 410(6830), 799–802, doi:10.1038/35071047, 2001.
- Butchart, N., Scaife, A. A., Bourqui, M., de Grandpré, J., Hare, S. H. E., Kettleborough, J., Langematz, U., Manzini, E., Sassi, F., Shibata, K., Shindell, D. and Sigmond, M.: Simulations of anthropogenic change in the strength of the Brewer–Dobson circulation, *Climate Dynamics*, 27(7–8), 727–741, doi:10.1007/s00382-006-0162-4, 2006.
- 550 Butchart, N., Cionni, I., Eyring, V., Shepherd, T. G., Waugh, D. W., Akiyoshi, H., Austin, J., Brühl, C., Chipperfield, M. P., Cordero, E., Dameris, M., Deckert, R., Dhomse, S., Frith, S. M., Garcia, R. R., Gettelman, A., Giorgetta, M. A., Kinnison, D. E., Li, F., Mancini, E., McLandress, C., Pawson, S., Pitari, G., Plummer, D. A., Rozanov, E., Sassi, F., Scinocca, J. F., Shibata, K., Steil, B. and Tian, W.: Chemistry–Climate Model Simulations of Twenty-First Century Stratospheric Climate and Circulation Changes, *Journal of Climate*, 23(20), 5349–5374, doi:10.1175/2010JCLI3404.1, 2010.
- 555 Calvo, N. and Garcia, R. R.: Wave Forcing of the Tropical Upwelling in the Lower Stratosphere under Increasing Concentrations of Greenhouse Gases, *Journal of the Atmospheric Sciences*, 66(10), 3184–3196, doi:10.1175/2009jas3085.1, 2009.
- Calvo, N., Garcia, R. R., Randel, W. J. and Marsh, D. R.: Dynamical Mechanism for the Increase in Tropical Upwelling in the
- 560 Lowermost Tropical Stratosphere during Warm ENSO Events, *Journal of the Atmospheric Sciences*, 67(7), 2331–2340, doi:10.1175/2010JAS3433.1, 2010.

- Chen, G., Lu, J. and Sun, L.: Delineating the Eddy–Zonal Flow Interaction in the Atmospheric Circulation Response to Climate Forcing: Uniform SST Warming in an Idealized Aquaplanet Model, *Journal of the Atmospheric Sciences*, 70(7), 2214–2233, doi:10.1175/JAS-D-12-0248.1, 2013.
- 565 Chiodo, G. and Polvani, L. M.: Reduced Southern Hemispheric circulation response to quadrupled CO<sub>2</sub> due to stratospheric ozone feedback, *Geophysical Research Letters*, 44(1), 465–474, doi:10.1002/2016GL071011, 2017.
- Chrysanthou, A., Maycock, A. C., Chipperfield, M. P., Dhomse, S., Garny, H., Kinnison, D., Akiyoshi, H., Deushi, M., Garcia, R. R., Jöckel, P., Kirner, O., Pitari, G., Plummer, D. A., Revell, L., Rozanov, E., Stenke, A., Tanaka, T. Y., Visioni, D. and Yamashita, Y.: The effect of atmospheric nudging on the stratospheric residual circulation in chemistry–climate  
570 models, *Atmospheric Chemistry and Physics*, 19(17), 11559–11586, doi:10.5194/acp-19-11559-2019, 2019.
- Cohen, N. Y., Gerber, E. P. and Bühler, O.: Compensation between Resolved and Unresolved Wave Driving in the Stratosphere: Implications for Downward Control, *Journal of the Atmospheric Sciences*, 70(12), 3780–3798, doi:10.1175/JAS-D-12-0346.1, 2013.
- Collins, M., Knutti, R., Arblaster, J., Dufresne, J.-L., Fichet, T., Friedlingstein, P., Gao, X., Gutowski, W. J., Johns, T. and  
575 Krinner, G.: Chapter 12 - Long-term Climate Change: Projections, Commitments and Irreversibility, in *Climate Change 2013 - The Physical Science Basis*, vol. 9781107057, edited by Intergovernmental Panel on Climate Change, pp. 1029–1136, Cambridge University Press, Cambridge., 2013.
- Deckert, R. and Dameris, M.: Higher tropical SSTs strengthen the tropical upwelling via deep convection, *Geophysical Research Letters*, 35(10), 2–5, doi:10.1029/2008GL033719, 2008.
- 580 Dickinson, R. E.: Planetary Rossby Waves Propagating Vertically Through Weak Westerly Wind Wave Guides, *Journal of the Atmospheric Sciences*, 25(6), 984–1002, doi:10.1175/1520-0469(1968)025<0984:PRWPVT>2.0.CO;2, 1968.
- Dobson, G. M. B.: Origin and distribution of the polyatomic molecules in the atmosphere, *Proceedings of the Royal Society of London. Series A. Mathematical and Physical Sciences*, 236(1205), 187–193, doi:10.1098/rspa.1956.0127, 1956.
- Dufresne, J.-L., Foujols, M.-A., Denvil, S., Caubel, A., Marti, O., Aumont, O., Balkanski, Y., Bekki, S., Bellenger, H.,  
585 Benschila, R., Bony, S., Bopp, L., Braconnot, P., Brockmann, P., Cadule, P., Cheruy, F., Codron, F., Cozic, A., Cugnet, D., de Noblet, N., Duvel, J.-P., Ethé, C., Fairhead, L., Fichet, T., Flavoni, S., Friedlingstein, P., Grandpeix, J.-Y., Guez, L., Guilyardi, E., Hauglustaine, D., Hourdin, F., Idelkadi, A., Ghattas, J., Joussaume, S., Kageyama, M., Krinner, G., Labetoulle, S., Lahellec, A., Lefebvre, M.-P., Lefebvre, F., Levy, C., Li, Z. X., Lloyd, J., Lott, F., Madec, G., Mancip, M., Marchand, M., Masson, S., Meurdesoif, Y., Mignot, J., Musat, I., Parouty, S., Polcher, J., Rio, C., Schulz, M.,  
590 Swingedouw, D., Szopa, S., Talandier, C., Terray, P., Viovy, N. and Vuichard, N.: Climate change projections using the IPSL-CM5 Earth System Model: from CMIP3 to CMIP5, *Climate Dynamics*, 40(9–10), 2123–2165, doi:10.1007/s00382-012-1636-1, 2013.
- Edmon, H. J., Hoskins, B. J. and McIntyre, M. E.: Eliassen-Palm Cross Sections for the Troposphere, *Journal of the Atmospheric Sciences*, 37(12), 2600–2616, doi:10.1175/1520-0469(1980)037<2600:EPCSFT>2.0.CO;2, 1980.
- 595 Eyring, V., Bony, S., Meehl, G. A., Senior, C. A., Stevens, B., Stouffer, R. J. and Taylor, K. E.: Overview of the Coupled

- Model Intercomparison Project Phase 6 (CMIP6) experimental design and organization, *Geoscientific Model Development*, 9(5), 1937–1958, doi:10.5194/gmd-9-1937-2016, 2016.
- 600 Fels, S. B., Mahlman, J. D., Schwarzkopf, M. D. and Sinclair, R. W.: Stratospheric Sensitivity to Perturbations in Ozone and Carbon Dioxide: Radiative and Dynamical Response, *Journal of the Atmospheric Sciences*, 37(10), 2265–2297, doi:10.1175/1520-0469(1980)037<2265:SSTPIO>2.0.CO;2, 1980.
- Flato, Gregory M., Marotzke, J. M. et al.: Chapter 9 - Evaluation of Climate Models, in *Climate Change 2013 - The Physical Science Basis*, vol. 9781107057, edited by Intergovernmental Panel on Climate Change, pp. 741–866, Cambridge University Press, Cambridge., 2013.
- 605 Fomichev, V. I., Jonsson, A. I., de Grandpré, J., Beagley, S. R., McLandress, C., Semeniuk, K. and Shepherd, T. G.: Response of the Middle Atmosphere to CO<sub>2</sub> Doubling: Results from the Canadian Middle Atmosphere Model, *Journal of Climate*, 20(7), 1121–1144, doi:10.1175/JCLI4030.1, 2007.
- Garcia, R. R. and Randel, W. J.: Acceleration of the Brewer–Dobson Circulation due to Increases in Greenhouse Gases, *Journal of the Atmospheric Sciences*, 65(8), 2731–2739, doi:10.1175/2008JAS2712.1, 2008.
- 610 Garfinkel, C. I., Waugh, D. W., Oman, L. D., Wang, L. and Hurwitz, M. M.: Temperature trends in the tropical upper troposphere and lower stratosphere: Connections with sea surface temperatures and implications for water vapor and ozone, *Journal of Geophysical Research: Atmospheres*, 118(17), 9658–9672, doi:10.1002/jgrd.50772, 2013.
- Garny, H., Dameris, M., Randel, W., Bodeker, G. E. and Deckert, R.: Dynamically Forced Increase of Tropical Upwelling in the Lower Stratosphere, *Journal of the Atmospheric Sciences*, 68(6), 1214–1233, doi:10.1175/2011JAS3701.1, 2011.
- 615 Hardiman, S. C., Butchart, N. and Calvo, N.: The morphology of the Brewer-Dobson circulation and its response to climate change in CMIP5 simulations, *Quarterly Journal of the Royal Meteorological Society*, 140(683), 1958–1965, doi:10.1002/qj.2258, 2014.
- Haynes, P. H., McIntyre, M. E., Shepherd, T. G., Marks, C. J. and Shine, K. P.: On the “Downward Control” of Extratropical Diabatic Circulations by Eddy-Induced Mean Zonal Forces, *Journal of the Atmospheric Sciences*, 48(4), 651–678, doi:10.1175/1520-0469(1991)048<0651:OTCOED>2.0.CO;2, 1991.
- 620 Hegglin, M. I. and Shepherd, T. G.: Large climate-induced changes in ultraviolet index and stratosphere-to-troposphere ozone flux, *Nature Geoscience*, 2(10), 687–691, doi:10.1038/ngeo604, 2009.
- Holton, J. R., Haynes, P. H., McIntyre, M. E., Douglass, A. R., Rood, R. B. and Pfister, L.: Stratosphere-troposphere exchange, *Reviews of Geophysics*, 33(4), 403, doi:10.1029/95RG02097, 1995.
- 625 Joshi, M. and Gregory, J.: Dependence of the land-sea contrast in surface climate response on the nature of the forcing, *Geophysical Research Letters*, 35(24), L24802, doi:10.1029/2008GL036234, 2008.
- Kawatani, Y., Hamilton, K. and Watanabe, S.: The Quasi-Biennial Oscillation in a Double CO<sub>2</sub> Climate, *Journal of the Atmospheric Sciences*, 68(2), 265–283, doi:10.1175/2010JAS3623.1, 2011.
- Keeble, J., Bednarz, E. M., Banerjee, A., Abraham, N. L., Harris, N. R. P., Maycock, A. C. and Pyle, J. A.: Diagnosing the radiative and chemical contributions to future changes in tropical column ozone with the UM-UKCA chemistry–climate

- 630 model, *Atmospheric Chemistry and Physics*, 17(22), 13801–13818, doi:10.5194/acp-17-13801-2017, 2017.
- Kim, B.-M., Son, S.-W., Min, S.-K., Jeong, J.-H., Kim, S.-J., Zhang, X., Shim, T. and Yoon, J.-H.: Weakening of the stratospheric polar vortex by Arctic sea-ice loss, *Nature Communications*, 5(1), 4646, doi:10.1038/ncomms5646, 2014.
- Kuhlbrodt, T., Jones, C. G., Sellar, A., Storkey, D., Blockley, E., Stringer, M., Hill, R., Graham, T., Ridley, J., Blaker, A., Calvert, D., Copsey, D., Ellis, R., Hewitt, H., Hyder, P., Ineson, S., Mulcahy, J., Siahahaan, A. and Walton, J.: The Low-Resolution Version of HadGEM3 GC3.1: Development and Evaluation for Global Climate, *Journal of Advances in Modeling Earth Systems*, 10(11), 2865–2888, doi:10.1029/2018MS001370, 2018.
- 635 Lamarque, J.-F., Bond, T. C., Eyring, V., Granier, C., Heil, A., Klimont, Z., Lee, D., Liousse, C., Mieville, A., Owen, B., Schultz, M. G., Shindell, D., Smith, S. J., Stehfest, E., Van Aardenne, J., Cooper, O. R., Kainuma, M., Mahowald, N., McConnell, J. R., Naik, V., Riahi, K. and van Vuuren, D. P.: Historical (1850–2000) gridded anthropogenic and biomass burning emissions of reactive gases and aerosols: methodology and application, *Atmospheric Chemistry and Physics*, 10(15), 7017–7039, doi:10.5194/acp-10-7017-2010, 2010.
- 640 Latif, M. and Keenlyside, N. S.: El Nino/Southern Oscillation response to global warming, *Proceedings of the National Academy of Sciences*, 106(49), 20578–20583, doi:10.1073/pnas.0710860105, 2009.
- Li, F., Stolarski, R. S. and Newman, P. A.: Stratospheric ozone in the post-CFC era, *Atmospheric Chemistry and Physics*, 9(6), 2207–2213, doi:10.5194/acp-9-2207-2009, 2009.
- 645 Lin, P. and Fu, Q.: Changes in various branches of the Brewer-Dobson circulation from an ensemble of chemistry climate models, *Journal of Geophysical Research: Atmospheres*, 118(1), 73–84, doi:10.1029/2012JD018813, 2013.
- Lin, P., Ming, Y. and Ramaswamy, V.: Tropical climate change control of the lower stratospheric circulation, *Geophysical Research Letters*, 42(3), 941–948, doi:10.1002/2014GL062823, 2015.
- 650 Manzini, E., Giorgetta, M. A., Esch, M., Kornbluh, L. and Roeckner, E.: The Influence of Sea Surface Temperatures on the Northern Winter Stratosphere: Ensemble Simulations with the MAECHAM5 Model, *Journal of Climate*, 19(16), 3863–3881, doi:10.1175/JCLI3826.1, 2006.
- Marsh, D. R. and Garcia, R. R.: Attribution of decadal variability in lower-stratospheric tropical ozone, *Geophysical Research Letters*, 34(21), L21807, doi:10.1029/2007GL030935, 2007.
- 655 Matsuno, T.: Vertical Propagation of Stationary Planetary Waves in the Winter Northern Hemisphere, *Journal of the Atmospheric Sciences*, 27(6), 871–883, doi:10.1175/1520-0469(1970)027<0871:vpospw>2.0.co;2, 1970.
- Maycock, A. C.: The contribution of ozone to future stratospheric temperature trends, *Geophysical Research Letters*, 43(9), 4609–4616, doi:10.1002/2016GL068511, 2016.
- McKenna, C. M., Bracegirdle, T. J., Shuckburgh, E. F., Haynes, P. H. and Joshi, M. M.: Arctic Sea Ice Loss in Different Regions Leads to Contrasting Northern Hemisphere Impacts, *Geophysical Research Letters*, 45(2), 945–954, doi:10.1002/2017GL076433, 2018.
- 660 McLandress, C. and Shepherd, T. G.: Simulated Anthropogenic Changes in the Brewer–Dobson Circulation, Including Its Extension to High Latitudes, *Journal of Climate*, 22(6), 1516–1540, doi:10.1175/2008JCLI2679.1, 2009.

- NCL: The NCAR Command Language (Version 6.6.2) [Software]. (2019). Boulder, Colorado: UCAR/NCAR/CISL/TDD.  
665 <http://dx.doi.org/10.5065/D6WD3XH5>, 2019.
- Nowack, P. J., Luke Abraham, N., Maycock, A. C., Braesicke, P., Gregory, J. M., Joshi, M. M., Osprey, A. and Pyle, J. A.: A large ozone-circulation feedback and its implications for global warming assessments, *Nature Climate Change*, 5(1), 41–45, doi:10.1038/nclimate2451, 2015.
- Olsen, M. A., Schoeberl, M. R. and Nielsen, J. E.: Response of stratospheric circulation and stratosphere-troposphere exchange  
670 to changing sea surface temperatures, *Journal of Geophysical Research*, 112(D16), D16104, doi:10.1029/2006JD008012, 2007.
- Oman, L., Waugh, D. W., Pawson, S., Stolarski, R. S. and Newman, P. A.: On the influence of anthropogenic forcings on changes in the stratospheric mean age, *Journal of Geophysical Research*, 114(D3), D03105, doi:10.1029/2008JD010378, 2009.
- 675 Plumb, R. A.: Stratospheric Transport, *Journal of the Meteorological Society of Japan. Ser. II*, 80(4B), 793–809, doi:10.2151/jmsj.80.793, 2002.
- Plumb, R. A. and Eluszkiewicz, J.: The Brewer–Dobson Circulation: Dynamics of the Tropical Upwelling, *Journal of the Atmospheric Sciences*, 56(6), 868–890, doi:10.1175/1520-0469(1999)056<0868:TBDCDO>2.0.CO;2, 1999.
- Randel, W. J., Garcia, R. and Wu, F.: Dynamical Balances and Tropical Stratospheric Upwelling, *Journal of the Atmospheric  
680 Sciences*, 65(11), 3584–3595, doi:10.1175/2008JAS2756.1, 2008.
- Randel, W. J., Garcia, R. R., Calvo, N. and Marsh, D.: ENSO influence on zonal mean temperature and ozone in the tropical lower stratosphere, *Geophysical Research Letters*, 36(15), n/a-n/a, doi:10.1029/2009GL039343, 2009.
- Rind, D., Suozzo, R., Balachandran, N. K. and Prather, M. J.: Climate Change and the Middle Atmosphere. Part I: The Doubled CO<sub>2</sub> Climate, *Journal of the Atmospheric Sciences*, 47(4), 475–494, doi:10.1175/1520-  
685 0469(1990)047<0475:CCATMA>2.0.CO;2, 1990.
- Rind, D., Lerner, J. and McLinden, C.: Changes of tracer distributions in the doubled CO<sub>2</sub> climate, *Journal of Geophysical Research: Atmospheres*, 106(D22), 28061–28079, doi:10.1029/2001JD000439, 2001.
- Rind, D., Lerner, J., Perlwitz, J., McLinden, C. and Prather, M.: Sensitivity of tracer transports and stratospheric ozone to sea surface temperature patterns in the doubled CO<sub>2</sub> climate, *Journal of Geophysical Research*, 107(D24), 4800,  
690 doi:10.1029/2002JD002483, 2002.
- Rosenlof, K. H.: Seasonal cycle of the residual mean meridional circulation in the stratosphere, *Journal of Geophysical Research*, 100(D3), 5173, doi:10.1029/94JD03122, 1995.
- Scaife, A. A., Butchart, N., Warner, C. D. and Swinbank, R.: Impact of a Spectral Gravity Wave Parameterization on the Stratosphere in the Met Office Unified Model, *Journal of the Atmospheric Sciences*, 59(9), 1473–1489, doi:10.1175/1520-0469(2002)059<1473:IOASGW>2.0.CO;2, 2002.
- 695 Semeniuk, K. and Shepherd, T. G.: Mechanisms for Tropical Upwelling in the Stratosphere, *Journal of the Atmospheric Sciences*, 58(21), 3097–3115, doi:10.1175/1520-0469(2001)058<3097:MFTUIT>2.0.CO;2, 2001.

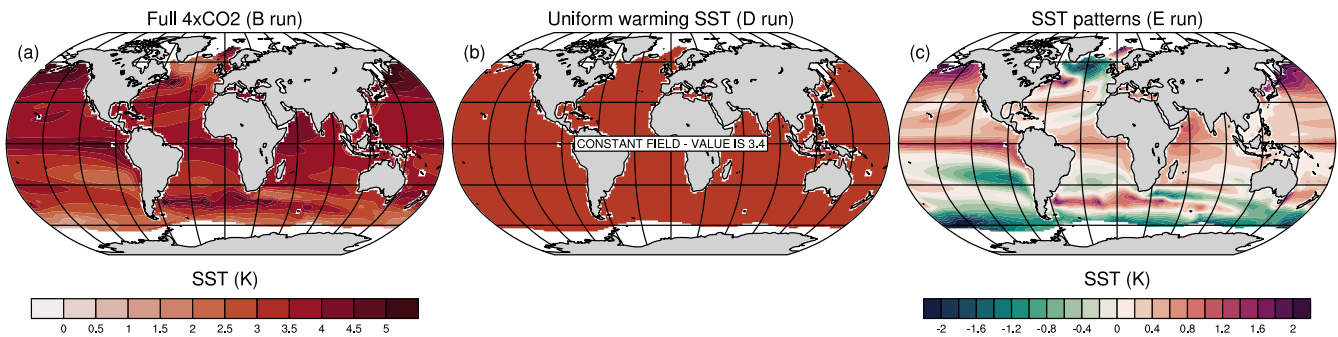
- 700 Shepherd, T. G. and McLandress, C.: A Robust Mechanism for Strengthening of the Brewer–Dobson Circulation in Response to Climate Change: Critical-Layer Control of Subtropical Wave Breaking, *Journal of the Atmospheric Sciences*, 68(4), 784–797, doi:10.1175/2010JAS3608.1, 2011.
- Sigmond, M. and Shepherd, T. G.: Compensation between Resolved Wave Driving and Parameterized Orographic Gravity Wave Driving of the Brewer–Dobson Circulation and Its Response to Climate Change, *Journal of Climate*, 27(14), 5601–5610, doi:10.1175/JCLI-D-13-00644.1, 2014.
- 705 Sigmond, M., Siegmund, P. C., Manzini, E. and Kelder, H.: A Simulation of the Separate Climate Effects of Middle-Atmospheric and Tropospheric CO<sub>2</sub> Doubling, *Journal of Climate*, 17(12), 2352–2367, doi:10.1175/1520-0442(2004)017<2352:ASOTSC>2.0.CO;2, 2004.
- Simpson, I. R., Shepherd, T. G. and Sigmond, M.: Dynamics of the Lower Stratospheric Circulation Response to ENSO, *Journal of the Atmospheric Sciences*, 68(11), 2537–2556, doi:10.1175/JAS-D-11-05.1, 2011.
- 710 SPARC: SPARC CCMVal Report on the Evaluation of Chemistry-Climate Models. V. Eyring, T. Shepherd and D. Waugh (Eds.), SPARC Report No. 5, WCRP-30/2010,WMO/TD-No.40 [online] Available from: <http://www.sparc-climate.org/publications/sparc-reports/sparc-report-no5/>, 2010.
- Taylor, K. E., Stouffer, R. J. and Meehl, G. A.: An Overview of CMIP5 and the Experiment Design, *Bulletin of the American Meteorological Society*, 93(4), 485–498, doi:10.1175/BAMS-D-11-00094.1, 2012.
- 715 Volodin, E. M.: The mechanism of multidecadal variability in the Arctic and North Atlantic in climate model INMCM4, *Environmental Research Letters*, 8(3), 035038, doi:10.1088/1748-9326/8/3/035038, 2013.
- Walters, D. N., Williams, K. D., Boutle, I. A., Bushell, A. C., Edwards, J. M., Field, P. R., Lock, A. P., Morcrette, C. J., Stratton, R. A., Wilkinson, J. M., Willett, M. R., Bellouin, N., Bodas-Salcedo, A., Brooks, M. E., Copsey, D., Earnshaw, P. D., Hardiman, S. C., Harris, C. M., Levine, R. C., MacLachlan, C., Manners, J. C., Martin, G. M., Milton, S. F., Palmer, M. D., Roberts, M. J., Rodríguez, J. M., Tennant, W. J. and Vidale, P. L.: The Met Office Unified Model Global Atmosphere 4.0 and JULES Global Land 4.0 configurations, *Geoscientific Model Development*, 7(1), 361–386, doi:10.5194/gmd-7-361-2014, 2014.
- 720 Webster, S., Brown, A. R., Cameron, D. R. and P. Jones, C.: Improvements to the representation of orography in the Met Office Unified Model, *Quarterly Journal of the Royal Meteorological Society*, 129(591), 1989–2010, doi:10.1256/qj.02.133, 2003.
- 725 Williams, K. D., Copsey, D., Blockley, E. W., Bodas-Salcedo, A., Calvert, D., Comer, R., Davis, P., Graham, T., Hewitt, H. T., Hill, R., Hyder, P., Ineson, S., Johns, T. C., Keen, A. B., Lee, R. W., Megann, A., Milton, S. F., Rae, J. G. L., Roberts, M. J., Scaife, A. A., Schiemann, R., Storkey, D., Thorpe, L., Watterson, I. G., Walters, D. N., West, A., Wood, R. A., Woollings, T. and Xavier, P. K.: The Met Office Global Coupled Model 3.0 and 3.1 (GC3.0 and GC3.1) Configurations, *Journal of Advances in Modeling Earth Systems*, 10(2), 357–380, doi:10.1002/2017MS001115, 2018.
- 730

Run ID	CO <sub>2</sub>	SSTs (prescribed)
A piControl	Pre-industrial	Pre-industrial
B Full 4×CO <sub>2</sub>	4×CO <sub>2</sub>	4×CO <sub>2</sub> (CMIP5)
C Atmos	4×CO <sub>2</sub>	Pre-industrial
D SST UW	Pre-industrial	4×CO <sub>2</sub> (UW) – 3.4 K
E SST patterns	Pre-industrial	4×CO <sub>2</sub> (patterns)
F SST UW low	Pre-industrial	Low 4×CO <sub>2</sub> – 2.1 K
G SST UW high	Pre-industrial	High 4×CO <sub>2</sub> – 4.9 K

**Table 1:** The sensitivity experiments used in this study with the atmospheric CO<sub>2</sub> and the SSTs used as boundary conditions. All other boundary conditions are as in piControl.

735

### Annual mean SST anomalies (K)



740

**Figure 1:** Prescribed annual-mean SST anomalies [K] with respect to the piControl climatology in the (a) full 4×CO<sub>2</sub>, (b) Uniform SST warming and (c) SST pattern perturbation experiments.

## Annual zonal mean T anomalies

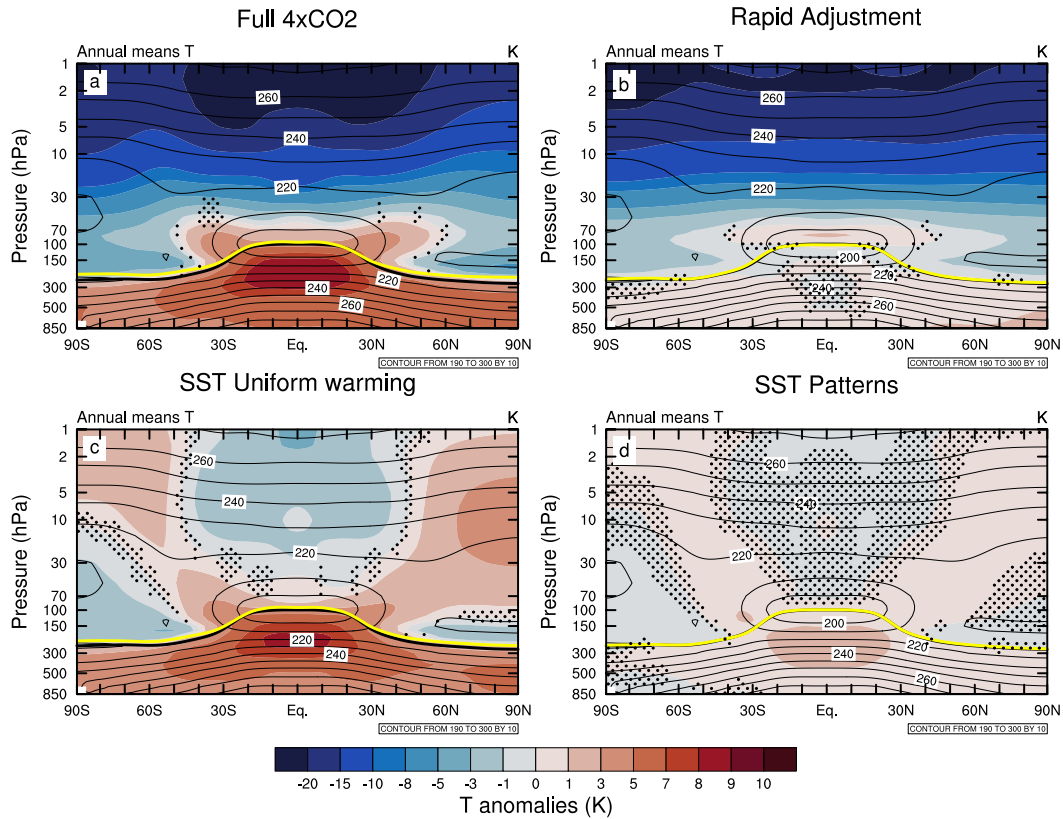


Figure 2: Latitude vs. pressure cross-sections of annual-mean and zonal-mean temperature anomalies [K] between 850–1 hPa with respect to the piControl simulation for the (a) 4xCO<sub>2</sub> (run B), (b) rapid adjustment (run C), (c) Uniform SST warming (run D) and (d) SST pattern (run E) experiments. Contours show the piControl climatology. Stippling denotes where the differences are not statistically significant at the 95% confidence level using a two-tailed Student's t test. Thick yellow and black lines indicate the tropopause pressure levels in each perturbation run and in the reference simulation, respectively.

745

750

## Annual Zonal mean u-wind anomalies

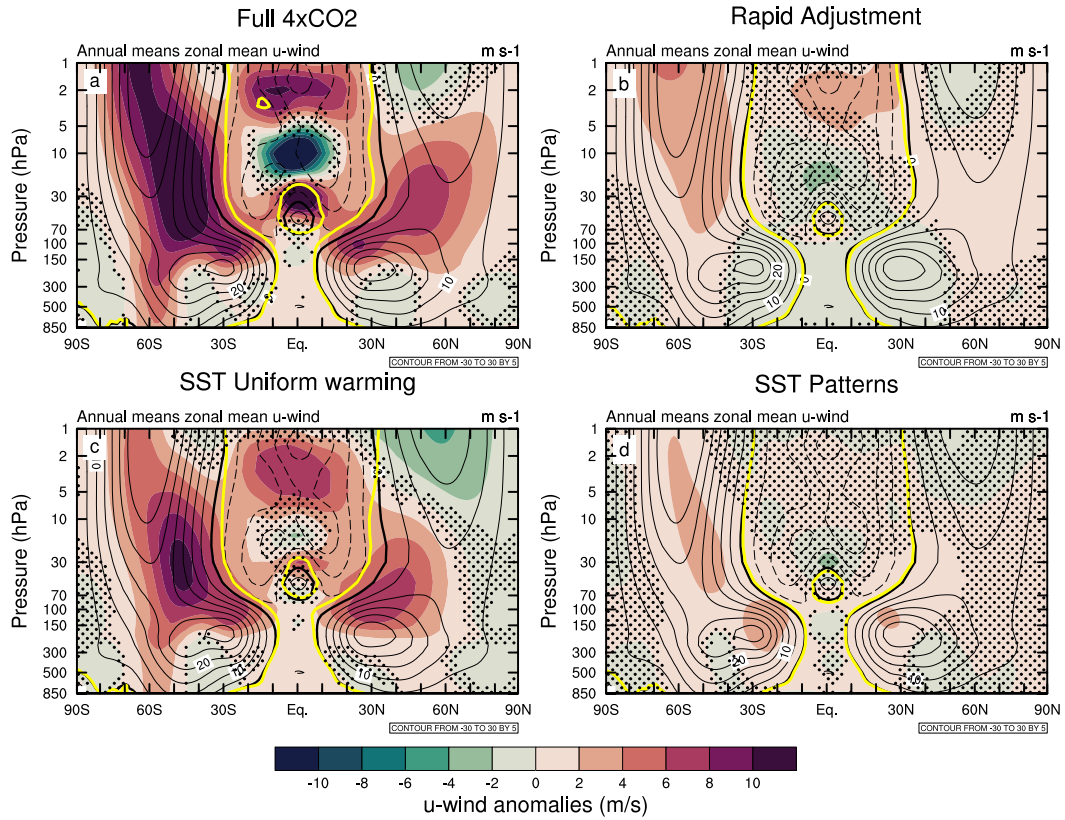


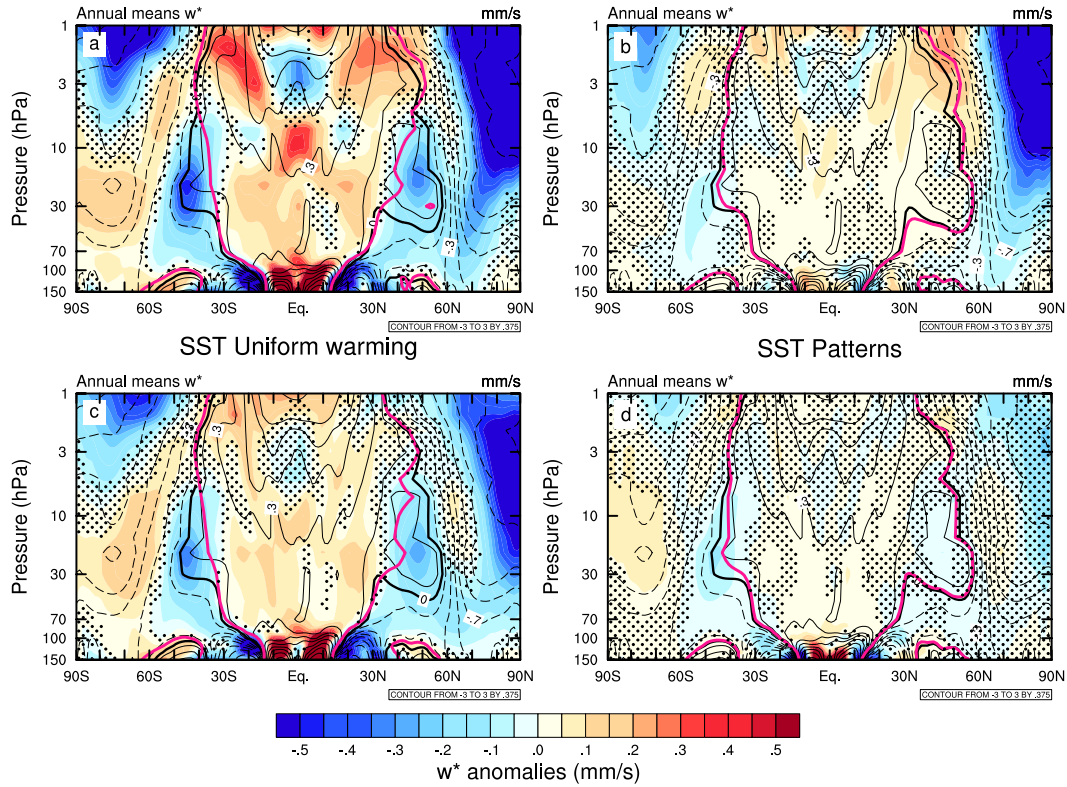
Figure 3: As in Figure 2, but for the annual and zonal-mean zonal wind anomalies [ $\text{m s}^{-1}$ ] between 850 – 1 hPa. Contours show the piControl climatology. The thick black lines denote the critical lines for stationary waves ( $\bar{u} = 0$ ) in piControl and the thick yellow lines for each perturbation experiment, respectively.

## Annual TEM vertical velocity anomalies

760

Full 4xCO<sub>2</sub>

Rapid Adjustment



765

770

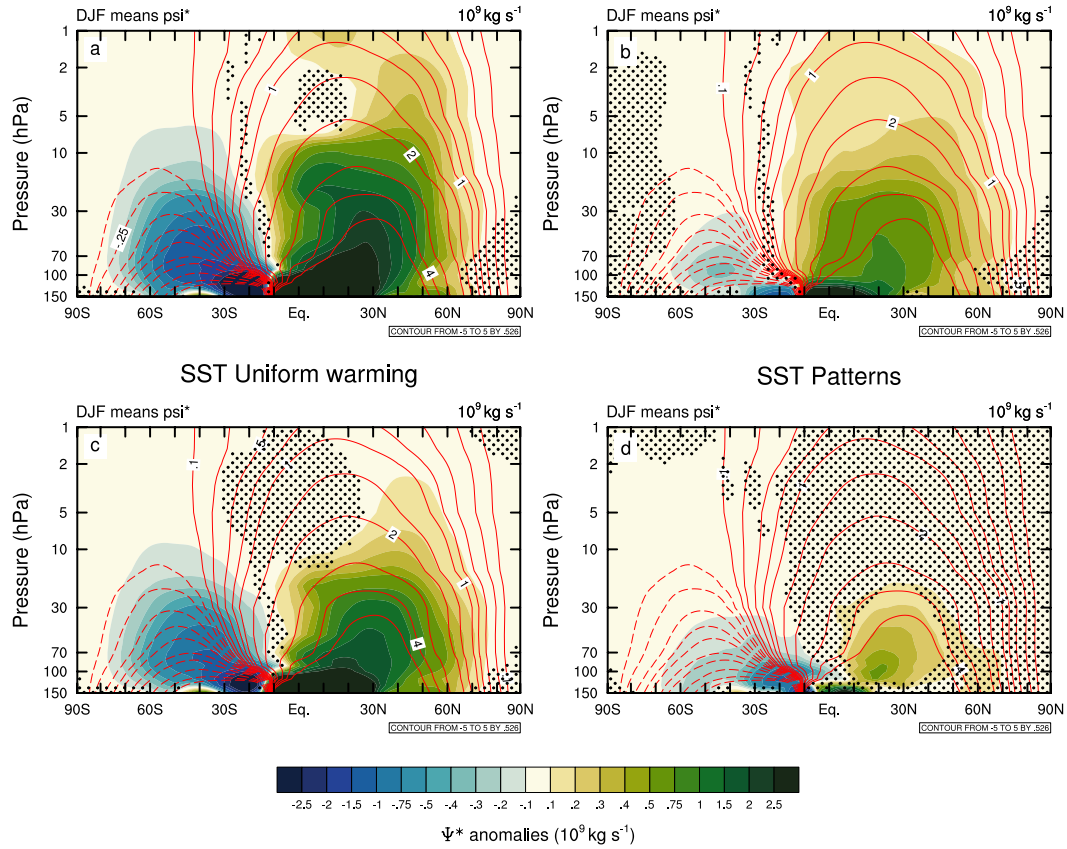
Figure 4: As in Figure 2, but for the annual-mean TEM residual vertical velocity anomalies [ $\text{mm s}^{-1}$ ] between 150–1 hPa. Contours show the piControl climatology and range from -3 to 3  $\text{mm s}^{-1}$  in increments of 0.375  $\text{mm s}^{-1}$ . The thick black lines denote the turnaround latitudes ( $\bar{w}^* = 0$ ) in piControl and pink thick lines for each perturbation experiment, respectively.

775

## DJF mean mass streamfunction anomalies

Full 4xCO<sub>2</sub>

Rapid Adjustment



780

785

790

Figure 5: DJF mean residual mass streamfunction anomalies [ $10^9 \text{ kg s}^{-1}$ ] between 150 – 1 hPa with respect to the piControl simulation for the (a)  $4\times\text{CO}_2$  (run B), (b) rapid adjustment (run C), (c) Uniform SST warming (run D) and (d) SST pattern (run E) experiments. Stippling denotes where the differences are not statistically significant at the 95% confidence level using a two-tailed Student's t test. Red contours plotted at  $-5, -4, -3, -2, -1.5, -1, -0.75, -0.5, -0.25, -0.1, 0.1, 0.25, 0.5, 0.75, 1, 1.5, 2, 3, 4$  and  $5 \times 10^9 \text{ kg s}^{-1}$  show the piControl climatology with negative values showed in dashed contours.

795

## JJA mean mass streamfunction anomalies

Full 4xCO<sub>2</sub>

Rapid Adjustment

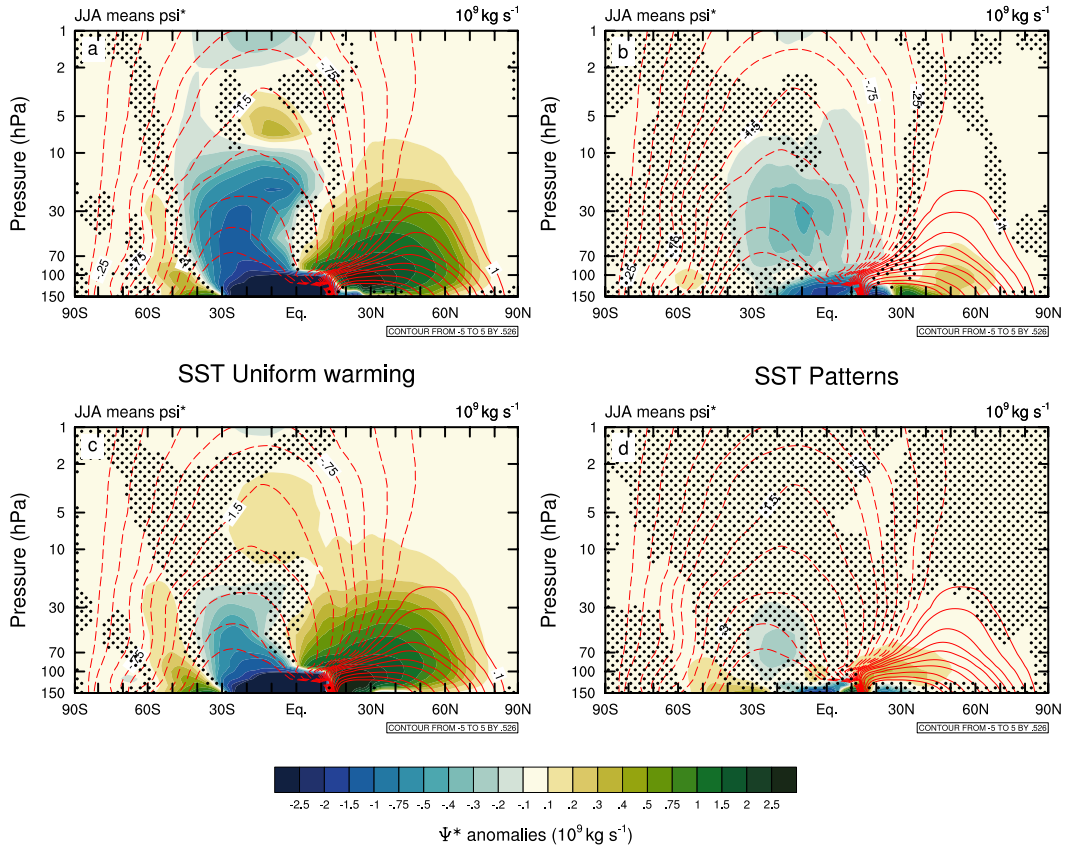


**Figure 6: As in Figure 5, but for the JJA season.**

**Figure 5: Annual mean residual mass streamfunction anomalies [ $10^9 \text{ kg s}^{-1}$ ] in the decomposed 4xCO<sub>2</sub> perturbation experiments. Stippling denotes where the differences are not statistically significant at the 95% confidence level. Red contours plotted at  $-5, -4, -3, -2, -1, -0.75, -0.25, 0.25, 0.75, 1, 2, 3, 4$  and  $5 \times 10^9 \text{ kg s}^{-1}$  show the piControl climatology with negative values showed in dashed contours.**

## DJF Divergence + EP Flux anomalies

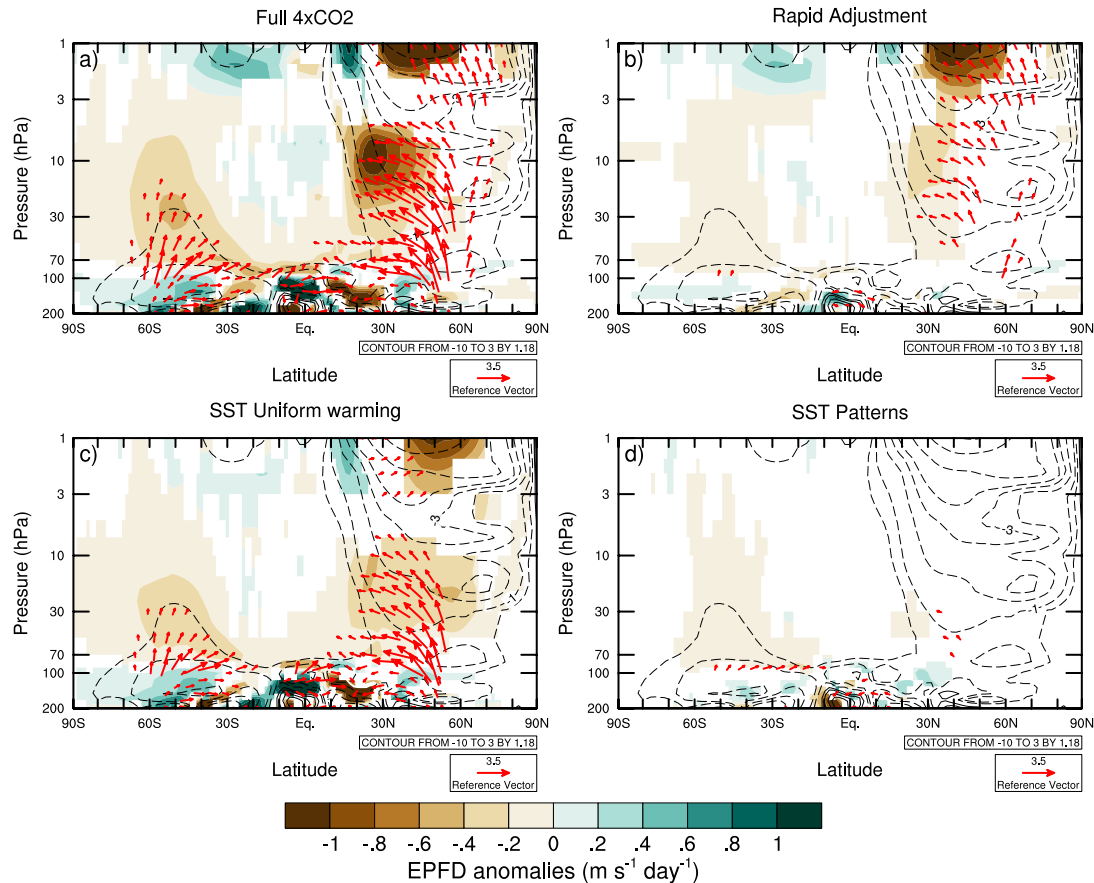


**Figure 67:** DJF average EP flux vector anomalies (red arrows) [ $\text{m}^2 \text{s}^{-2}$ ] and EP flux divergence anomalies [ $\text{m s}^{-1} \text{day}^{-1}$ ] (shading) between 200 – 1 hPa with respect to the piControl simulation for the (a) 4xCO<sub>2</sub> (run B), (b) rapid adjustment (run C), (c) Uniform SST warming (run D) and (d) SST pattern (run E) experiments in the decomposed 4xCO<sub>2</sub> experiments. The EPF divergence here is multiplied by the cosine of latitude to represent the torque exerted on the zonal flow. Contours show the piControl climatology with contours plotted at -10, -8, -6, -4, -3, -2, -1, -0.5, 0.5, 1, 2, 3 m s<sup>-1</sup> day<sup>-1</sup>. The EP flux vector and divergence anomalies are only plotted where they are significant at the 95% confidence level using a two-tailed Student's t test. The EP flux vectors have been scaled following Edmon et al. (1980) and were scaled by a magnification factor of 5 in the stratosphere in order to enhance their visibility.

825

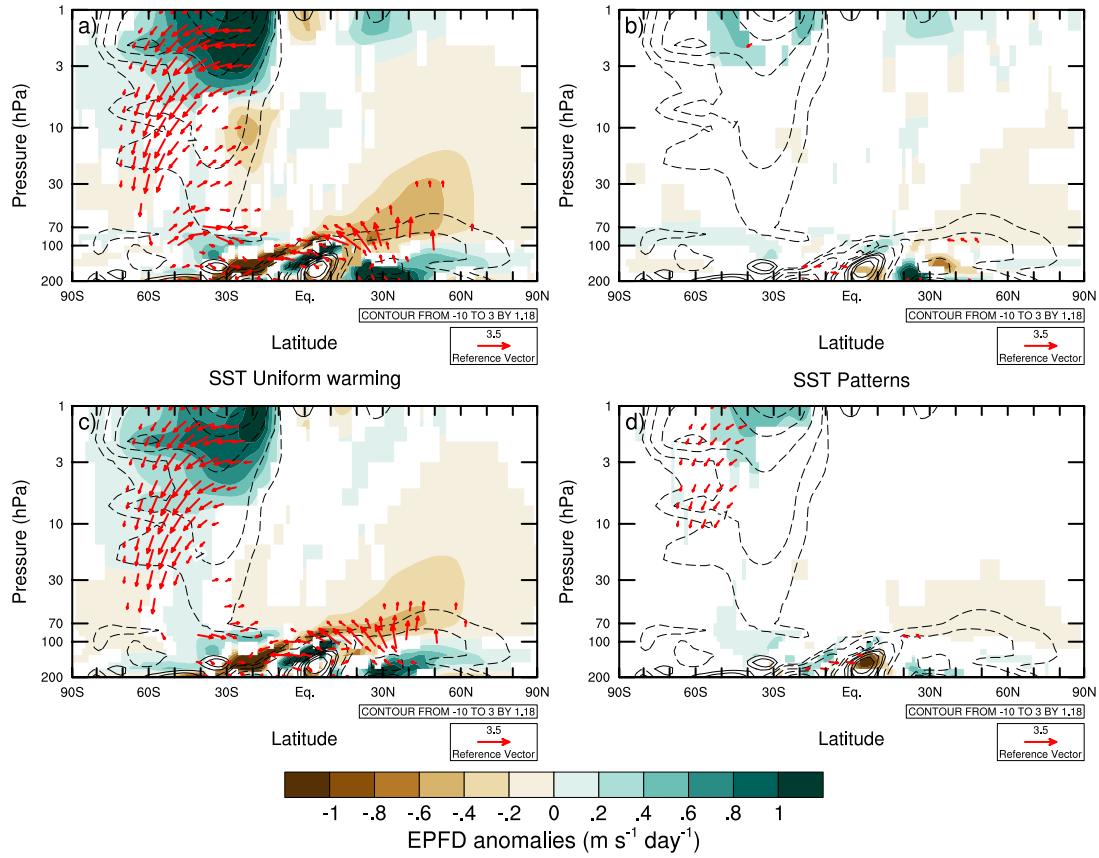
830

|

### JJA Divergence + EP Flux anomalies

Full 4xCO<sub>2</sub>

Rapid Adjustment



840

845

850 **Figure 78:** As in Figure 67, but for the JJA season.

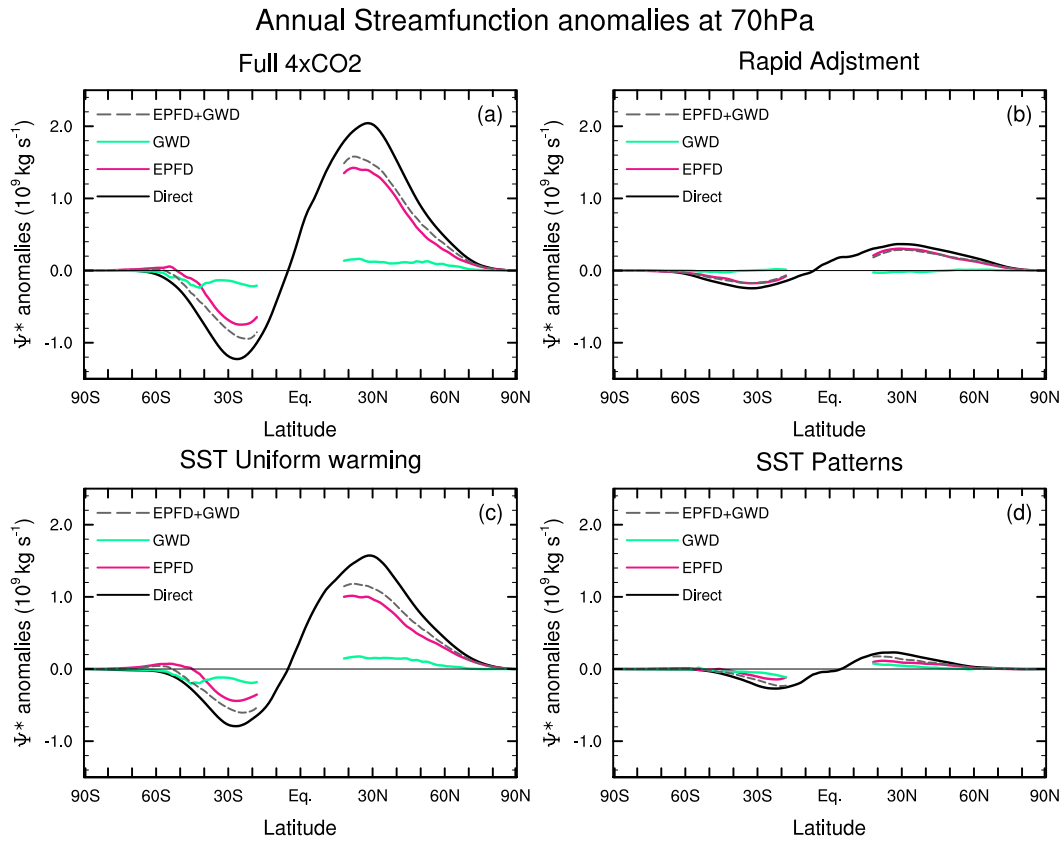


**Figure 89:** Annual-mean residual streamfunction anomalies [ $10^9 \text{ kg s}^{-1}$ ] at 70 hPa with respect to the piControl simulation for the (a)  $4\times\text{CO}_2$  (run B), (b) rapid adjustment (run C), (c) Uniform SST warming (run D) and (d) SST pattern (run E) experiments.

855 Black line shows the direct calculation, the downward control calculations for EPFD, OGWD + NOGWD and their sum (EPFD + OGWD + NOGWD) are shown in magenta, green and grey dashed, respectively.

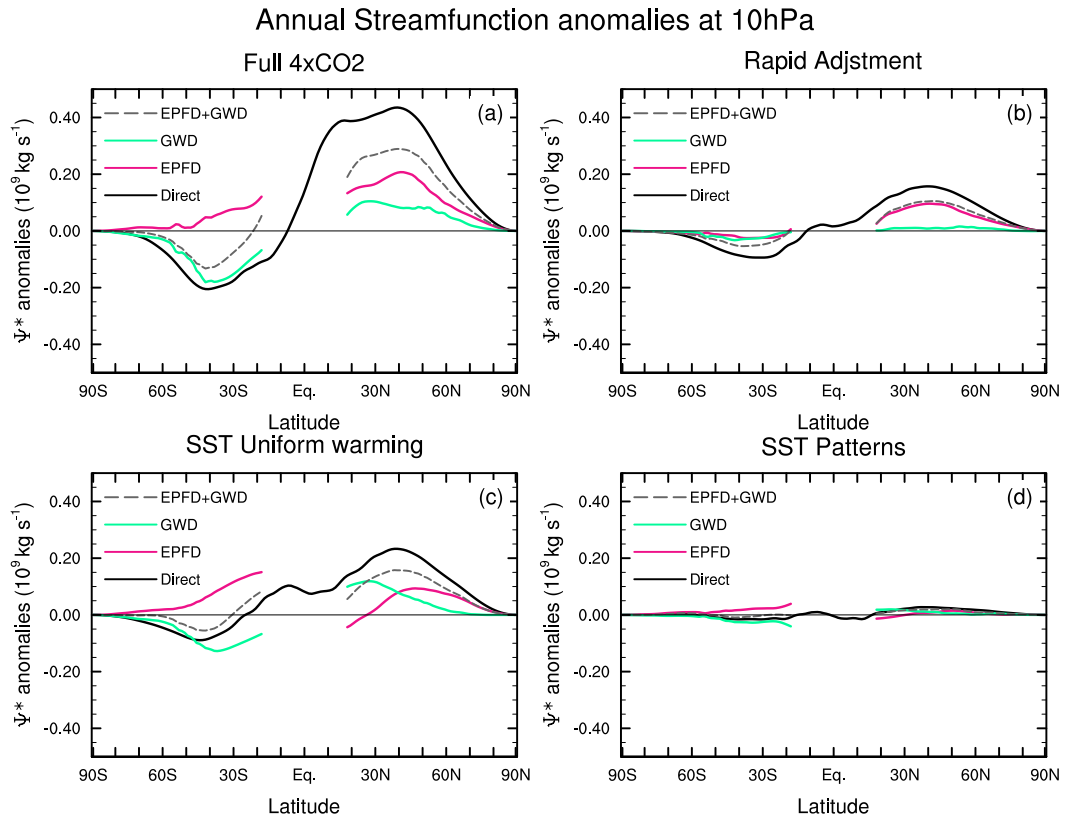


Figure 910: As in Figure 89, but at 10 hPa.

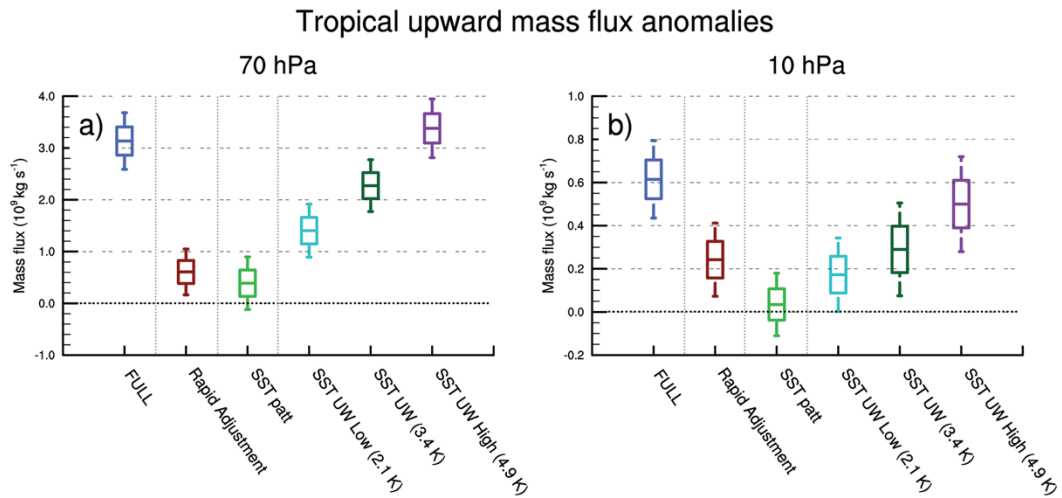


Figure 1011: Annual-mean tropical upward mass flux anomalies [ $10^9 \text{ kg s}^{-1}$ ] at (a) 70 hPa and (b) 10 hPa in the different perturbation experiments as labelled. The edges of the boxplots indicate  $\pm 1$  standard deviation of the interannual variability and the whiskers indicate  $\pm 2$  standard deviations.

*Supplement of*

## **Decomposing the response of the stratospheric Brewer-Dobson circulation to an abrupt quadrupling in CO<sub>2</sub>**

Chrysanthou et al.

---

---

<i>CMIP5 Models</i>				
1. ACCESS1-0	2. ACCESS1-3	3. CCSM4	4. CNRM-CM5	5. CSIRO-Mk3-6-0
6. CanESM2	7. EC-EARTH	8. GFDL-CM3	9. GFDL-ESM2G	10. GFDL-ESM2M
11. GISS-E2-H	12. GISS-E2-R	13. HadGEM2-ES	14. IPSL-CM5A-LR	15. IPSL-CM5A-MR
16. IPSL-CM5B-LR	17. MIROC-ESM	18. MIROC5	19. MPI-ESM-LR	20. MPI-ESM-MR
21. MPI-ESM-P	22. MRI-CGCM3	23. NorESM1-M	24. BCC-CSM1-1-M	25. BCC-CSM1-1
26. INMCM4				

---

---

**Table S1: The CMIP5 global coupled ocean-atmosphere general circulation models used to construct the SST and SIC boundary conditions in this study.**

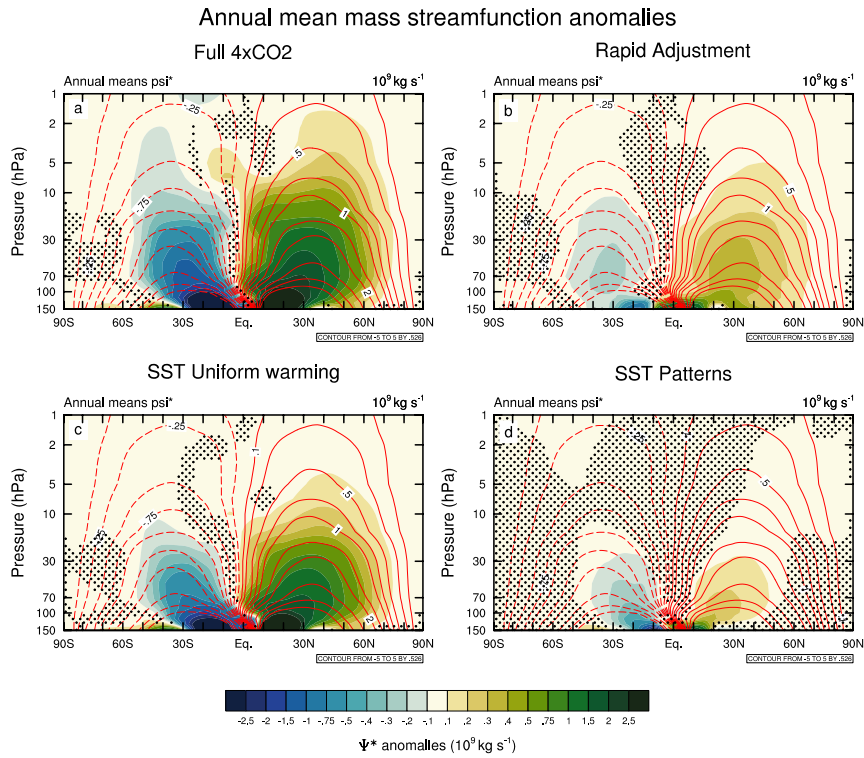


**Figure S1: Annual mean residual mass streamfunction anomalies [ $10^9 \text{ kg s}^{-1}$ ] between 150 – 1 hPa with respect to the piControl simulation for the (a) 4xCO<sub>2</sub> (run B), (b) rapid adjustment (run C), (c) Uniform SST warming (run D) and (d) SST pattern (run E) experiments. Stippling denotes where the differences are not statistically significant at the 95% confidence level using a two-tailed Student's t test. Red contours plotted at -5, -4, -3, -2, -1.5, -1, -0.75, -0.5, -0.25, -0.1, 0.1, 0.25, 0.5, 0.75, 1, 1.5, 2, 3, 4 and  $5 \times 10^9 \text{ kg s}^{-1}$  show the piControl climatology with negative values showed in dashed contours.**

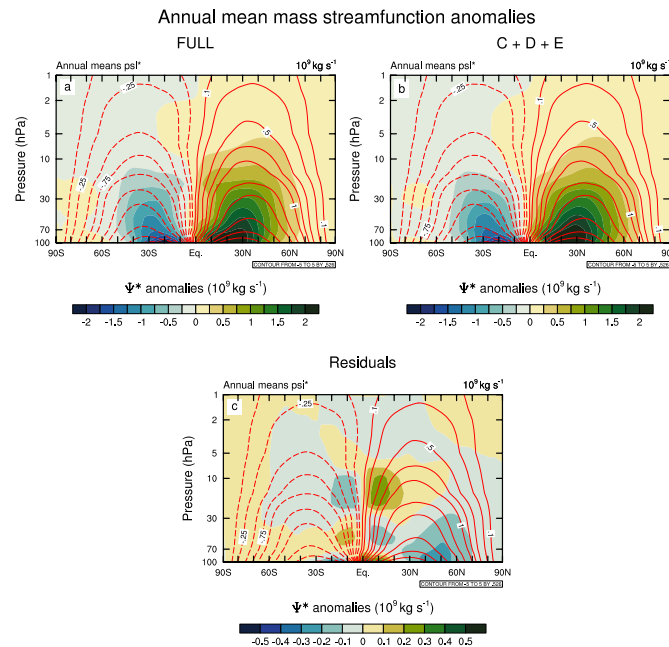


**Figure S2: The residual mass streamfunction anomalies [ $10^9 \text{ kg s}^{-1}$ ] in (a) the full 4xCO<sub>2</sub> experiment (as in Fig. 5a), (b) the sum of experiments C+D+E and (c) a – b differences. Note panel (c) has a different colour scale. This shows the decomposition of the streamfunction response in the full experiment into the three components analysed in the main text works to leading order.**



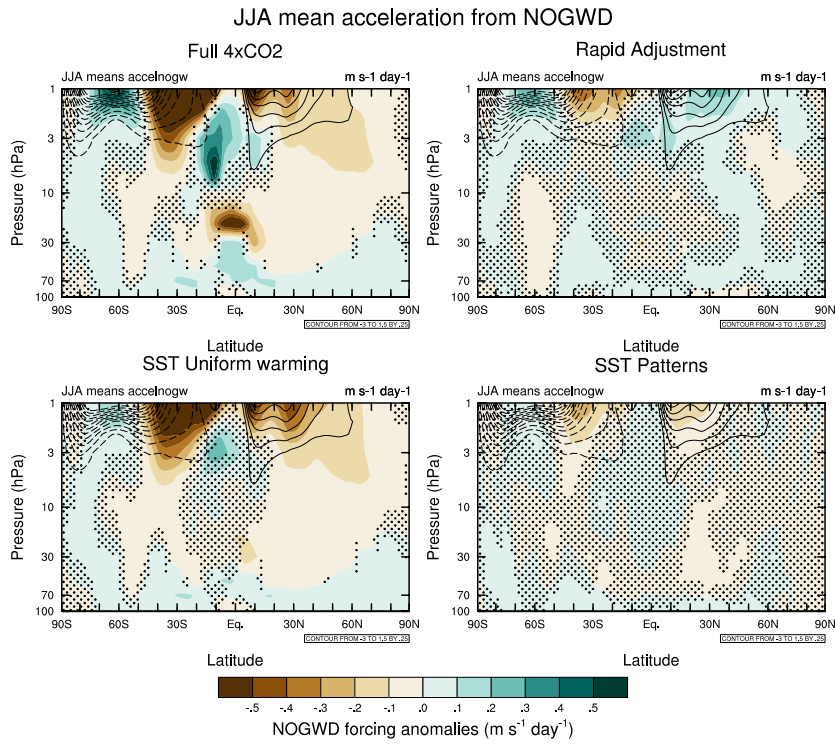


**Figure S5:** As in Figure S4, but for JJA.

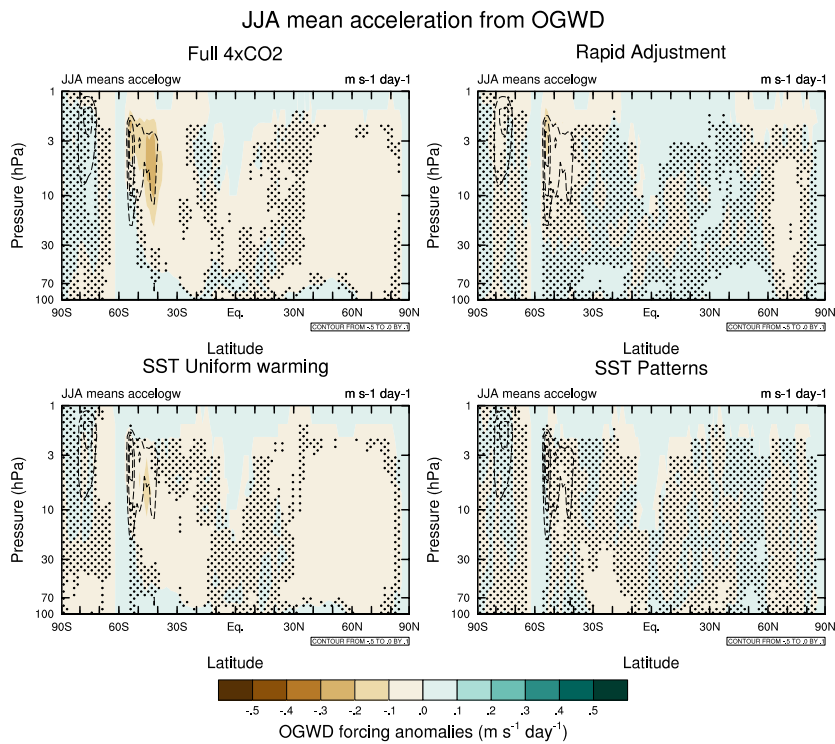


**Figure S6:** As in Figure S5, but for JJA.